Lack of *Tgfbr1* and *Acvr1b* synergistically stimulates myofibre hypertrophy and accelerates muscle regeneration

M.M.G. Hillege[1]*, A. Shi[1,2,3]*, R.A. Galli[1], G. Wu[2,4], P. Bertolino[5], W.M.H. Hoogaars[1,6], R.T. Jaspers[1#]

1. Laboratory for Myology, Department of Human Movement Sciences, Faculty of Behavioural and Movement Sciences, Vrije Universiteit Amsterdam, Amsterdam Movement Sciences, Amsterdam, The Netherlands
2. Department of Oral and Maxillofacial Surgery/Pathology, Amsterdam UMC and Academic Center for Dentistry Amsterdam (ACTA), Vrije Universiteit Amsterdam (VU), Amsterdam Movement Sciences, Amsterdam, the Netherlands
3. Department of Prosthodontics, Affiliated Stomatology Hospital of Guangzhou Medical University, Guangdong Engineering Research Center of Oral Restoration and Reconstruction, Guangzhou Key Laboratory of Basic and Applied Research of Oral Regenerative Medicine, Guangzhou, China
4. Department of Oral Cell Biology, Academic Centre for Dentistry Amsterdam (ACTA), University of Amsterdam and Vrije Universiteit Amsterdam, Amsterdam Movement Sciences, Amsterdam, the Netherlands
5. Centre de Recherche en Cancérologie de Lyon, UMR INSERM U1052/CNRS 5286, Université de Lyon, Centre Léon Bérard, Lyon, France
6. European Research Institute for the Biology of Ageing (ERIBA), University Medical Center Groningen (UMCG), University of Groningen, Groningen, The Netherlands

*Contributed equally to this manuscript

[#]Correspondence: r.t.jaspers@vu.nl; Tel.: +31 (0) 205988463

Abstract

In skeletal muscle, transforming growth factor-β (TGF-β) family growth factors, TGF-β1 and myostatin, are involved in atrophy and muscle wasting disorders. Simultaneous interference with their signalling pathways may improve muscle function, however little is known about their individual and combined receptor signalling. Here we show that inhibition of TGF-β signalling by simultaneous muscle-specific knockout of TGF-β type I receptors *Tgfbr1* and *Acvr1b* simultaneously, induces substantial hypertrophy, while such effect does not occur by single receptor knockout. Hypertrophy is induced by increased phosphorylation of Akt and p70S6K and reduced E3 ligases expression, while myonuclear number remains unaltered. Combined knockout of both TGF-β type I receptors increases the number of satellite cells, macrophages and improves regeneration post cardiotoxin-induced injury by stimulating myogenic differentiation. Extra cellular matrix gene expression is exclusively elevated in muscle with combined receptor knockout. *Tgfbr1* and *Acvr1b* are synergistically involved in regulation of myofibre size, regeneration and collagen deposition.

Key words: TGF-β; Myostatin; Type I receptor; Cardiotoxin; Injury; Inflammation; Fibrosis; Hypertrophy; Skeletal muscle

43 **Introduction**

44 Muscle wasting disorders, such as muscular dystrophies, cancer cachexia and sarcopenia are
45 characterised by reduced muscle mass, impaired regeneration and fibrosis, which results in
46 progressive muscle weakness. The transforming growth factor β (TGF-β) superfamily members
47 TGF-β1, myostatin and activin A are involved in various processes within muscle tissue and
48 overexpression of these proteins contributes to muscle wasting pathologies (Bernasconi et al.,
49 1995; Carlson, Hsu, & Conboy, 2008; J. L. Chen et al., 2014; Costelli et al., 2008; Leger,
50 Derave, De Bock, Hespel, & Russell, 2008; Tanaka, Miyazaki, Takeda, & Takeo, 1993).

51 TGF-β signalling negatively affects muscle growth by both affecting satellite cells (SCs)
52 and myofibres. TGF-β1, myostatin and activin A inhibit myoblast differentiation (Langley et
53 al., 2002; Liu, Black, & Derynck, 2001; Trendelenburg, Meyer, Jacobi, Feige, & Glass, 2012).
54 Inhibition of myostatin and activin A synergistically results in muscle hypertrophy (Amirouche
55 et al., 2009; J. L. Chen et al., 2017; J. L. Chen et al., 2014; Latres et al., 2017; McFarlane et al.,
56 2006; Zimmers et al., 2002). These effects are at least partly independent of SCs (Lee et al.,
57 2012). In addition, TGF-β1 overexpression *in vivo* may also cause muscle atrophy (Mendias et
58 al., 2012; Narola, Pandey, Glick, & Chen, 2013).

59 Transient TGF-β1 expression may play an essential role during muscle regeneration.
60 TGF-β1 is expressed by inflammatory cells, such as macrophages, monocytes and neutrophils
61 as well as by fibroblasts after acute injury (Assoian et al., 1987; Grotendorst, Smale, & Pencev,
62 1989; Lawrence, Pircher, Kryceve-Martinerie, & Jullien, 1984; Zimowska et al., 2009). During
63 muscle regeneration, TGF-β1 is involved in the regulation of the immune response and plays
64 an important role in rebuilding extracellular matrix (ECM) (Gillies & Lieber, 2011; Kehrl et
65 al., 1986; Reibman et al., 1991; Tsunawaki, Sporn, Ding, & Nathan, 1988; Wahl et al., 1987;
66 Wiseman, Polverini, Kamp, & Leibovich, 1988). However, chronic increased expression of
67 TGF-β is known to contribute to muscle fibrosis (Y. Li et al., 2004). Furthermore, myostatin

68 and activin A have also been suggested to induce substantial skeletal muscle fibrosis (J. L. Chen
69 et al., 2014; Z. B. Li, Kollias, & Wagner, 2008). Thus, inhibition of TGF-β signalling in the
70 myofibre may substantially reduce connective tissue deposition.

71 In animal models, such as murine X-linked muscular dystrophy (mdx) mice, a Duchenne
72 muscular dystrophy (DMD) mouse model, cancer cachexia mouse models or aged mice,
73 inhibiting signalling of one or more of these ligands had beneficial effects, such as reduction in
74 fibrosis and maintenance of muscle mass (Andreetta et al., 2006; J. L. Chen et al., 2017; Greco
75 et al., 2015; Latres et al., 2015; K. T. Murphy et al., 2011). Lack of either TGF-β or myostatin
76 has been suggested to improve regeneration after acute injury (Accornero et al., 2014;
77 McCroskery et al., 2005). Therefore, inhibiting these growth factors may be a promising
78 therapeutic strategy to alleviate muscle wasting pathologies.

79 However, interference with signalling of TGF-β family members may be complicated.
80 TGF-β family members regulate various cellular processes throughout the body, thus systemic
81 inhibition of these growth factors may have severe consequences. Furthermore, due to overlap
82 in function of these ligands, inhibition of a single ligand is likely not effective.

83 Simultaneous inhibition of TGF-β1, myostatin and activin A through interference with
84 their downstream receptors may be an effective approach. The TGF-β family consists of at least
85 33 cytokines that can roughly be divided into the TGF-β/myostatin/activins subgroup and the
86 growth differentiation factor/bone morphogenetic protein (BMP) group that often have
87 opposing effects. These cytokines regulate gene expression via specific binding to distinct type
88 II and type I receptors. TGF-β1 mainly signals via the type II receptor, TGF-β receptor type-2
89 (TGFBR2), and via the type I receptor, TGF-β receptor type-1 (TGFBR1 or ALK5). Myostatin
90 signals via the type II receptor, activin receptor type-2B (ACVR2B), and activin A signals via
91 type II receptors, activin receptor type-2A (ACVR2A) and ACVR2B. Activin A signals via
92 type I receptor, activin receptor type-1B (ACVR1B or ALK4). Myostatin has been shown to

93 signal via both TGFBR1 and ACVR1B in various cell types (Kemaladewi et al., 2012;
94 Rebbapragada, Benchabane, Wrana, Celeste, & Attisano, 2003; ten Dijke et al., 1994).

95 Interference with myostatin/activin A signalling by blocking their type II receptors
96 ACVR2A/B may not be an appropriate strategy, since these receptors are also involved in BMP
97 signalling, which stimulates muscle hypertrophy whereas myostatin/activin A signalling is
98 associated with atrophy (Sartori, Gregorevic, & Sandri, 2014; Tsuchida, Nakatani, Uezumi,
99 Murakami, & Cui, 2008). Moreover, interference with signalling via these receptors may cause
100 severe side effects, such as nose and gum bleeds, as has been shown in in DMD boys treated
101 with soluble ACVR2B (Campbell et al., 2017). Inhibition of type I receptors TGFBR1 and
102 ACVR1B may provide a more specific and effective approach to alleviate muscle wasting
103 pathologies (Sartori et al., 2014; Tsuchida et al., 2008). However, very little is known about the
104 role of these receptors in the regulation of skeletal muscle mass and regeneration.

105 The aim of this study was to obtain insight in how myofibre specific knockout of type I
106 receptors *Tgfbr1* and *Acvr1b* affected muscle size as well as early muscle regeneration,
107 inflammation and collagen deposition in both intact and injured muscle. We hypothesised that
108 individual knockout of these TGF-β type I receptors would have marginal effects. Moreover,
109 simultaneous inhibition of these type I receptors would substantially increase muscle size and
110 enhanced early myofibre regeneration, while attenuating fibrosis.

111 **Results**

112 *Acvr1b* and *Tgfbr1* expression was successfully reduced after tamoxifen treatment

113 The aim of this study was to investigate effects of mature myofibre specific knockout of *Tgfbr1*
114 and *Acvr1b* on muscle morphology as well as early muscle regeneration, inflammation and
115 collagen deposition in both uninjured muscle tissue and after acute cardiotoxin (CTX) injury.
116 For this purpose, the HSA-MCM mouse line (McCarthy, Srikuea, Kirby, Peterson, & Esser,
117 2012b), that expresses tamoxifen (TMX) inducible Cre (MerCreMer) under a human α-skeletal
118 actin (HSA) promotor was cross bred with the conditional knockout Acvr1b$^{fl/fl}$ (Ripoche et al.,
119 2013) and Tgfbr1$^{fl/fl}$ (Larsson et al., 2001) mouse lines to obtain mouse lines HSA-
120 MCM:Acvr1b$^{fl/fl}$, HSA-MCM:Tgfbr1$^{fl/fl}$ and HSA-MCM:Acvr1b$^{fl/fl}$:Tgfbr1$^{fl/fl}$ (further referred
121 to as Acvr1b$^{fl/fl}$, Tgfbr1$^{fl/fl}$ and Acvr1b$^{fl/fl}$:Tgfbr1$^{fl/fl}$). Receptors were deleted when mice were
122 6 weeks old (Figure 1A and B).

123 Expression levels of *Acvr1b* and *Tgfbr1* mRNA showed successful knockout as *Acvr1b*
124 mRNA levels in tibialis anterior (TA) muscles were reduced in Acvr1b$^{fl/fl}$ animals by 97% and
125 in Acvr1b$^{fl/fl}$:Tgfbr1$^{fl/fl}$ animals by 88%. *Tgfbr1* expression levels in TA muscles were reduced
126 in Tgfbr1$^{fl/fl}$ animals by 82% Unexpectedly, *Tgfbr1* expression levels in TA muscle of
127 Acvr1b$^{fl/fl}$:Tgfbr1$^{fl/fl}$ animals were not significantly reduced compared to those of control
128 animals (Figure 1C). Note, however, that lack of significantly reduced *Tgfbr1* expression is
129 likely a consequence of high *Tgfbr1* expression by other cell types present within the muscle,
130 rather than unsuccessful knockdown. This issue is addressed below in more detail (see Figure
131 3). *Acvr1b* expression levels did not affect *Tgfbr1* expression levels and vice versa.

132

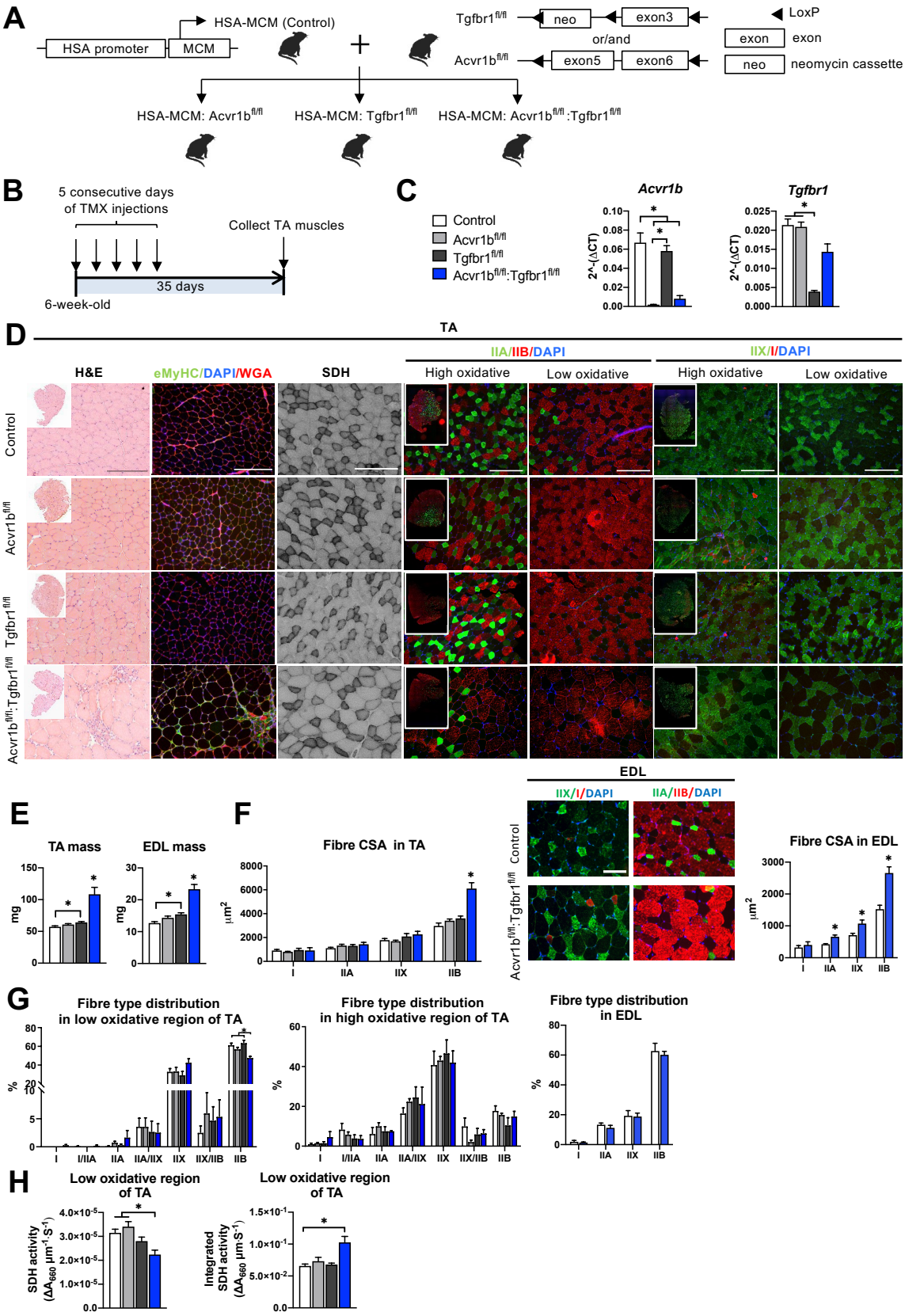

Figure 1. Simultaneous knockout of both *Acvr1b* and *Tgfbr1* caused muscle hypertrophy. (A) Scheme showing cross-breeding of HSA-MCM mouse line with conditional knockout mouse

136 lines Acvr1b$^{fl/fl}$ and Tgfbr1$^{fl/fl}$. LoxP sites are indicated by black arrows. A loxP-flanked
137 neomycin (neo) cassette is inserted upstream of exon3 of Acvr1b genome. (B) Scheme
138 demonstrating receptor knockout induced by tamoxifen (TMX) injection for consecutive 5
139 days. (C) Relative mRNA expression of *Acvr1b* and *Tgfbr1* in TA muscles of experimental
140 groups. (D) Histology stainings of TA muscles 35 day after first TMX injection. H&E staining
141 and immunofluorescent staining of eMyHC (green) of TA showed regenerative regions
142 containing eMyHC^{+} myofibres with central nuclei (DAPI, blue) in Acvr1b$^{fl/fl}$:Tgfbr1$^{fl/fl}$ mice,
143 wheat glucose agglutinin (WGA, red) was used to visualise cell membranes and ECM.
144 Acvr1b$^{fl/fl}$:Tgfbr1$^{fl/fl}$ mice showed lower staining intensity for SDH in low oxidative region of
145 TA. MyHCs staining demonstrated type IIA (green), IIB (red), IIX (green) and I (red) myofibres
146 in low and high oxidative regions of TA. Scale bars=250 µm. (E) TA and EDL muscle masses
147 and myofibre cross-sectional areas (CSAs) were increased in Acvr1b$^{fl/fl}$:Tgfbr1$^{fl/fl}$ mice. (F) In
148 TA, specifically CSA of type IIB myofibres was increased in Acvr1b$^{fl/fl}$:Tgfbr1$^{fl/fl}$ animals,
149 while in EDL CSA of all type II myofibres was increased. Myofibre types were stained in EDL.
150 (G) Percentage of type IIB in low oxidative region of TA was reduced. No differences were
151 observed in myofibre distribution in high oxidative region of TA or EDL. (H) SDH activity
152 (absorbance units (ΔA_{660}) per micrometer section thickness per second of incubation time
153 ($\Delta A_{660} \cdot \mu m^{-1} \cdot s^{-1}$)) was decreased, while the integrated SDH activity SDH activity multiplied by
154 CSA ($\Delta A_{660} \cdot \mu m \cdot s^{-1}$) increased in low oxidative region of TA of Acvr1b$^{fl/fl}$:Tgfbr1$^{fl/fl}$ animals.
155 N=5-8 mice. Results are presented as mean + SEM. *: $P < 0.05$. Significant difference between
156 individual groups is indicated by lines with a *. Single * indicates significant difference
157 compared to all other groups.
158

159 Simultaneous knockout of *Acvr1b* and *Tgfbr1* resulted in type IIB myofibre hypertrophy and
160 has modest effects on myofibre type distribution
161 TGFBR1 and ACVR1B ligands are well known for their regulatory effects on muscle mass.
162 Here, TA mass of Acvr1b$^{fl/fl}$:Tgfbr1$^{fl/fl}$ mice (108.4 ± 11.0 mg) was nearly doubled compared
163 to that of control animals (57.2 ± 1.5 mg). TA mass of Tgfbr1$^{fl/fl}$ mice (64.2 ± 1.4 mg) was also
164 increased, however to a much lower extend. TA mass of Acvr1b$^{fl/fl}$ mice (60.8 ± 1.5 mg) did
165 not differ from that of controls (Figure 1E). To test whether the observed effects in TA also
166 apply to other muscles, extensor digitorum longus muscle (EDL) mass was determined. Similar
167 to TA muscle, EDL mass of Acvr1b$^{fl/fl}$:Tgfbr1$^{fl/fl}$ (23.3 ± 1.5 mg) and Tgfbr1^{flfl} mice (15.4 ± 0.5
168 mg) was increased by 1.8-fold and 1.3-fold, compared to that of control mice (12.7 ± 0.4 mg),
169 respectively, while EDL mass of Acvr1b$^{fl/fl}$ mice (14.4 ± 0.5 mg) did not differ from that of
170 control mice (Figure 1E). Note that in TA, specifically the cross-sectional area (CSA) of type
171 IIB myofibres of Acvr1b$^{fl/fl}$:Tgfbr1$^{fl/fl}$ mice was twofold larger compared to that of control
172 animals (Figure 1F), indicating that simultaneous knockout of both *Acvr1b* and *Tgfbr1*
173 synergistically causes myofibre hypertrophy in type IIB myofibres. In contrast to observations
174 in TA, CSA of type IIA and type IIX myofibres in EDL muscle of Acvr1b$^{fl/fl}$:Tgfbr1$^{fl/fl}$ mice
175 were increased by 1.6-fold and 1.5-fold compared to those of control mice, respectively.
176 However, similar to TA muscle, CSA of type IIB myofibres of Acvr1b$^{fl/fl}$:Tgfbr1$^{fl/fl}$ mice was
177 increased most substantially compared to that of control mice (1.7-fold) (Figure 1F).
178 These results indicate that simultaneous knockout of *Acvr1b* and *Tgfbr1* in mature mouse
179 myofibre synergistically causes muscle hypertrophy of mostly type IIB myofibres, whereas
180 individual knockout has little effect on muscle mass or myofibre CSA.
181 Observed effects on myofibre CSA may indicate alterations in myofibre metabolism as
182 well as in myofibre type distribution. Therefore, myofibre type distribution was determined in
183 both the high and low oxidative region of the TA (Figure 1D and G). In the high oxidative

184 region no significant differences were observed. However, in the low oxidative region of
185 Acvr1b$^{fl/fl}$:Tgfbr1$^{fl/fl}$ animals the percentage of type IIB myofibres was lower (47 ± 2%)
186 compared to both control (61 ± 2%) and Tgfbr1^{flfl} animals (63 ± 3%) (Figure 1G), which
187 indicates a shift towards an oxidative phenotype in these muscles. In contrast, no differences in
188 EDL myofibre type distribution were observed between Acvr1b$^{fl/fl}$:Tgfbr1$^{fl/fl}$ and control mice
189 (Figure 1F and G).

190 Taken together, lack of both *Acvr1b* and *Tgfbr1* reduces the percentage of type IIB
191 myofibres in TA muscle, but has only modest effects on myofibre type distribution.

192

193 Type IIB myofibre hypertrophy resulted in reduced SDH activity

194 In skeletal muscle, myofibre size and oxidative capacity are inversely related, indicating that
195 metabolism implies a size constraint (W. van der laarse, Tombe, Groot, & Diegenbach, 1997;
196 van Wessel, de Haan, van der Laarse, & Jaspers, 2010). To test whether the excessive
197 hypertrophy within the low oxidative region of the TA muscles was accompanied by a reduction
198 in oxidative metabolism, succinate dehydrogenase (SDH) activity and integrated SDH activity
199 were determined. In Acvr1b$^{fl/fl}$:Tgfbr1$^{fl/fl}$ mice SDH activity was decreased by 30% compared
200 to that in Acvr1b$^{fl/fl}$ and control animals. However, the integrated SDH activity (total oxidative
201 capacity of myofibres) in Acvr1b$^{fl/fl}$:Tgfbr1$^{fl/fl}$ mice was increased by 60% compared to that in
202 control animals. This suggests that while locally the total oxidative capacity in the low oxidative
203 region of TA muscle of Acvr1b$^{fl/fl}$:Tgfbr1$^{fl/fl}$ animals may be reduced, the oxidative capacity
204 per myofibre in the low oxidative region of TA muscle of these animals was substantially
205 increased (Figure 1H).

206

207 Myofibres with central nuclei and increased number of SCs were observed in TA muscle of
208 Acvr1b$^{fl/fl}$:Tgfbr1$^{fl/fl}$ mice

209 Hematoxylin & Eosin (H&E) staining and embryonic myosin heavy chain (eMyHC) staining
210 showed within TA of uninjured Acvr1b$^{fl/fl}$:Tgfbr1$^{fl/fl}$ animals, regions with small myofibres
211 with centrally located nuclei, indicating injured myofibres. These myofibres were eMyHC^{+} and
212 surrounded by many other cells, likely a combination of SCs, fibroblasts and immune cells
213 (Figure 1D). These regions with regenerating myofibres were mainly present in the low
214 oxidative region of the TA and comprised on average 2.95% of the muscle CSA. These regions
215 were almost never observed in TA of other animals (<0.2%) (Figure 2A). Similar regions with
216 myofibres containing centrally located myonuclei were also observed in EDL (1.45% of the
217 muscle CSA) of Acvr1b$^{fl/fl}$:Tgfbr1$^{fl/fl}$ animals and not in EDL of control animals (0.08%)
218 (Figure 2A). Together, these data indicate that simultaneous knockout of *Acvr1b* and *Tgfbr1*
219 results in spontaneous damage and regeneration. Spontaneous regeneration requires activation
220 of SCs. In the low oxidative region of TA muscle of Acvr1b$^{fl/fl}$:Tgfbr1$^{fl/fl}$ animals the number
221 of SCs per myofibre in a cross-section was increased compared to that in control animals
222 (Figure 2B).

223 We next characterised cells surrounding the spontaneously regenerating regions in TA
224 as being macrophages or fibroblasts. F4/80 staining showed that the number of macrophages
225 per mm^2 muscle CSA in Acvr1b$^{fl/fl}$:Tgfbr1$^{fl/fl}$ animals was increased by 14-fold (23.7
226 cells/mm^2) compared to that in control (1.7 cells/mm^2) and Acvr1b$^{fl/fl}$ animals (1.7 cells/mm^2),
227 while in Tgfbr1$^{fl/fl}$ animals (4.5 cells/mm^2) the number of macrophages per mm^2 did not differ
228 compared to that in the other three groups (Figure 2C).

229 Taken together, in TA and EDL muscles that lack both *Acvr1b* and *Tgfbr1* regions with
230 spontaneously regenerating myofibres were observed. These regions are accompanied by an
231 increased number of SCs and macrophages.

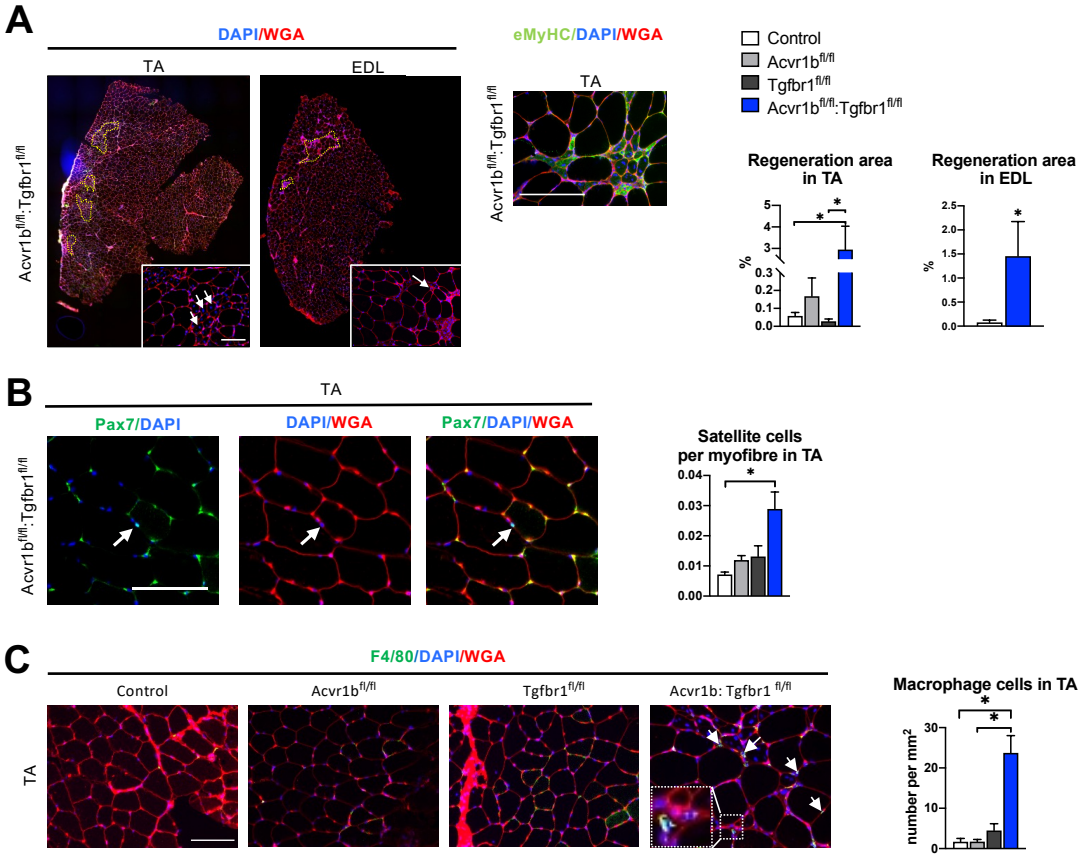

232

233 **Figure 2.** Increased heterogeneity of cell types was found in both TA and EDL of
234 Acvr1b$^{fl/fl}$:Tgfbr1$^{fl/fl}$ animals. (A) Regions with spontaneously regenerating myofibres (circled
235 by yellow dash lines) with central nuclei (indicated by arrows) were particularly present in low
236 oxidative region of TA and EDL of Acvr1b$^{fl/fl}$:Tgfbr1$^{fl/fl}$ animals. (B) Increased number of
237 Pax7^{+} cells per myofibre was found in TA of Acvr1b$^{fl/fl}$:Tgfbr1$^{fl/fl}$ mice. (C) IF staining of F4/80
238 (green) showed an increased number of macrophages (indicated by arrows) in TA muscle per
239 mm^2 CSA of Acvr1b$^{fl/fl}$:Tgfbr1$^{fl/fl}$ mice compared to control. Macrophages (image with higher
240 magnification on the left corner) were mainly located around myofibres with central nuclei.
241 Scale bar indicates 100 µm. N=5-8 mice. Results are presented as mean + SEM. *. $P < 0.05$.
242 Significant difference between individual groups is indicated by lines with a *. Single *
243 indicates significant difference compared to all other groups at the same time point.

244

245 Lack of both *Acvr1b* and *Tgfbr1* in the skeletal myofibre increased *Hgf* expression levels and
246 Akt/p70S6K signalling, while decreasing *Murf-1* expression levels
247 Next, we aimed to obtain insight in the mechanisms underlying the increase in
248 Acvr1b$^{fl/fl}$:Tgfbr1$^{fl/fl}$ TA mass and myofibre CSA, as well as the observed increase in SC
249 number and regeneration regions in these muscles. First, we determined whether the increase
250 in myofibre size was accompanied by accretion of myonuclei. Counts of myonuclear fragments
251 in muscle cross-sections of IIB myofibres did not differ between control and
252 Acvr1b$^{fl/fl}$:Tgfbr1$^{fl/fl}$ animals. Moreover, in longitudinal sections no difference in length of
253 myonuclei per myofiber was found between groups (Figure 3A), which indicates that the
254 probability to encounter a myonucleus within a cross-section was equal between groups. The
255 excessive hypertrophy of type IIB myofibres of Acvr1b$^{fl/fl}$:Tgfbr1$^{fl/fl}$ mice occurred without
256 accretion of myonuclei and caused a 70% increase in the myonuclear domain (Figure 3A).
257 Phosphorylation of TGF-β type I receptor is known to activate canonical Smad2/3
258 signalling. Therefore, we examined the effects of TGF-β type I receptor knockout on Smad2/3
259 phosphorylation in both TA and EDL muscle (Figure 3B). Single knockout did not affect
260 phosphorylated / total protein ratios for Smad2 and Smad3 in muscles of Acvr1b$^{fl/fl}$ or Tgfbr1$^{fl/fl}$
261 mice, which was in line with the lack of effect on muscle size and phenotype and suggested that
262 at least the presence of one of the two receptors was sufficient to maintain the Smad signalling.
263 With regard to Smad2/3 phosphorylation in TA and EDL of Acvr1b$^{fl/fl}$:Tgfbr1$^{fl/fl}$ mice, a 31%
264 reduction was shown for phosphorylation of Smad2 in EDL while phosphorylated levels of
265 Smads2 and 3 tended to be reduced in TA
266 Since receptors were specifically knocked out in skeletal myofibres, other cell types
267 such as SCs, fibroblasts or inflammatory cells remained sensitive to TGF-β signalling.
268 Therefore, the effect of receptor knockout on *Tgf-β1* and myostatin (*Mstn*) expression were
269 determined. In TA muscles of Acvr1b$^{fl/fl}$:Tgfbr1$^{fl/fl}$ animals, *Tgf-β1* expression levels were 2.2-

270 fold higher compared to those of control animals, while *Tgf-β1* expression levels of Acvr1b$^{fl/fl}$
271 and Tgfbr1$^{fl/fl}$ animals did not differ from those of control animals. *Mstn* expression levels
272 within Acvr1b$^{fl/fl}$:Tgfbr1$^{fl/fl}$ mice were only increased compared to those of Acvr1b$^{fl/fl}$ animals
273 (Figure 3C). These results indicate that lack of both *Tgfbr1* and *Acvr1b* in skeletal myofibres
274 resulted in increased *Tgf-β1* expression in muscle tissue, which may be associated with an
275 enhanced local regeneration.

276 Expression levels of various growth factors, i.e. insulin-like growth factor 1Ea (*Igf1ea),*
277 mechano growth factor *(Mgf),* fibroblast growth factor 2 (*Fgf-2*)*,* hepatocyte growth factor
278 (*Hgf*), interleukin-6 (*Il-6*) and vascular endothelial growth factor (*Vegf*) may contribute to SC
279 proliferation or myofibre size (Arsic et al., 2004; Coleman et al., 1995; Lefaucheur & Sebille,
280 1995; Pedersen, Steensberg, & Schjerling, 2001; Serrano, Baeza-Raja, Perdiguero, Jardi, &
281 Munoz-Canoves, 2008; Tatsumi, Anderson, Nevoret, Halevy, & Allen, 1998; Yang &
282 Goldspink, 2002). No significant differences were observed in expression levels of *Igf1ea, Il-6*
283 or *Fgf-2*. *Mgf* expression levels in TA muscle of Acvr1b$^{fl/fl}$:Tgfbr1$^{fl/fl}$ animals were reduced
284 compared to those of Acvr1b$^{fl/fl}$ or control animals. *Vegf* expression levels of
285 Acvr1b$^{fl/fl}$:Tgfbr1$^{fl/fl}$ animals were reduced compared to those of all other groups, while *Vegf*
286 levels of Tgfbr1$^{fl/fl}$ animals were reduced compared to those of control animals. In contrast, *Hgf*
287 expression levels of Acvr1b$^{fl/fl}$:Tgfbr1$^{fl/fl}$ animals were increased compared to those of all other
288 groups (Figure 3C). These results suggest that in TA muscle of Acvr1b$^{fl/fl}$:Tgfbr1$^{fl/fl}$ animals
289 enhanced expression of *Hgf* may contribute to the observed increase in SC number and
290 myofibre hypertrophy.

291 Myostatin and activin A both have been shown to reduce protein synthesis by decreasing
292 phosphorylation of Akt and its downstream target p70S6 kinase (p70S6K) (Amirouche et al.,
293 2009; J. L. Chen et al., 2014; McFarlane et al., 2006; Trendelenburg et al., 2009). In TA muscle
294 of Acvr1b$^{fl/fl}$:Tgfbr1$^{fl/fl}$ animals, phosphorylated Akt had increased by 2.3-fold compared to that

295 of control animals. A similar but insignificant trend was observed for total Akt relative intensity.
296 No significant differences in the phosphorylated Akt/total Akt ratio were observed. However,
297 phosphorylated p70S6K had increased by 1.9-fold compared to that of control animals, while
298 total p70S6K was not significantly affected. As a consequence, the phosphorylated
299 p70S6K/total p70S6K was increased by 1.7-fold (Figure 3D). Together, these results indicate
300 simultaneous knockout of *Acvr1b* and *Tgfbr1* in skeletal myofibre stimulates that the protein
301 synthesis via activation of Akt/mTOR/p70S6K signalling.

302 Finally, myostatin and TGF-β1 have been indicated to stimulate muscle specific E3
303 ubiquitin ligases muscle RING-finger protein-1 (MuRF-1) and atrogin-1. *Murf-1*expression
304 levels in TA muscles of Acvr1b$^{fl/fl}$:Tgfbr1$^{fl/fl}$ mice were significantly lower compared to those
305 of Acvr1b$^{fl/fl}$ or control animals. *Atrogin-1* expression did not differ between groups (Figure
306 3C). Together, these results indicate that simultaneous knockout of *Acvr1b* and *Tgfbr1* in
307 skeletal myofibre reduces protein breakdown via suppression of *Murf-1* expression.

308

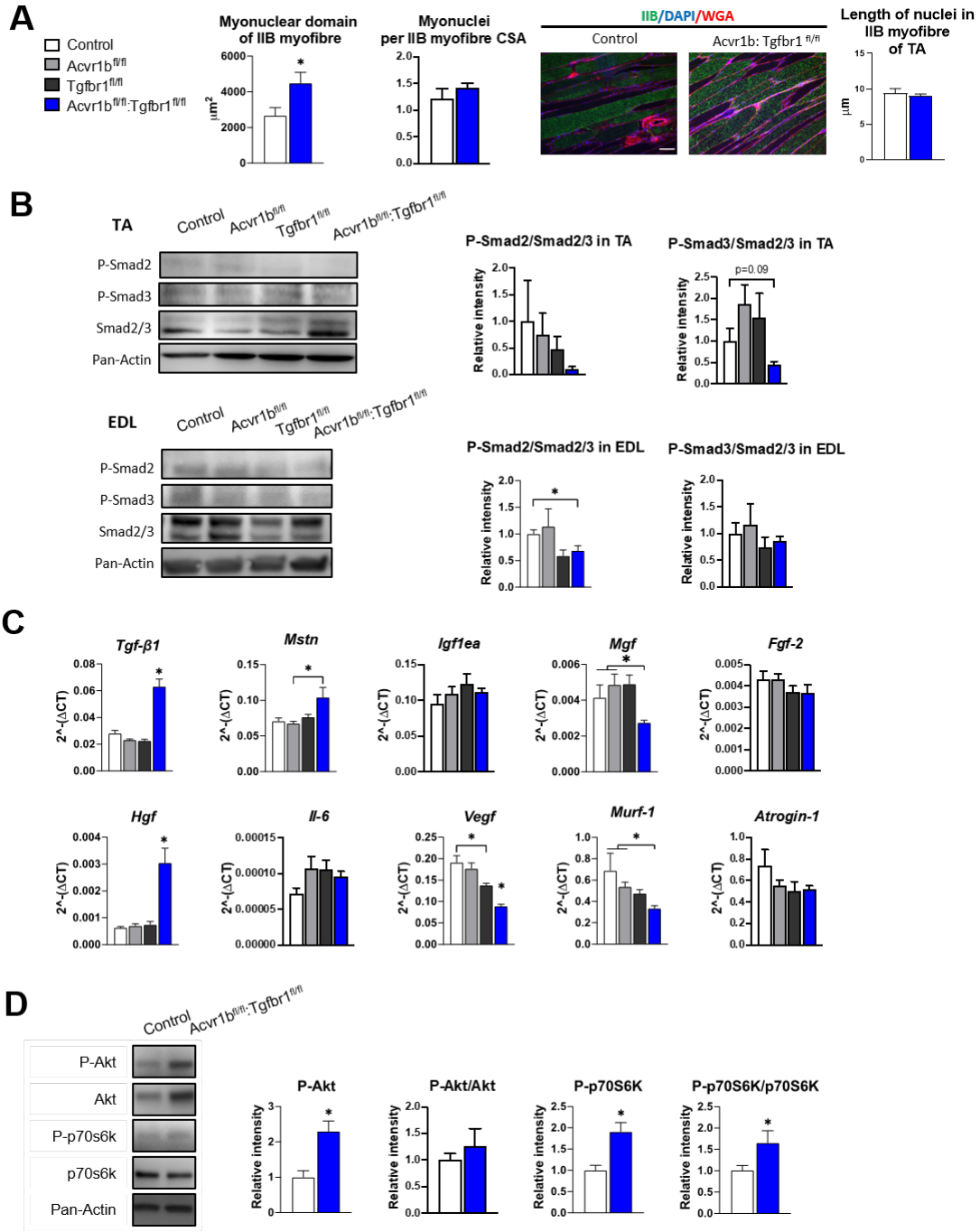

309

310 **Figure 3.** Effects of simultaneous knockout of both *Acvr1b* and *Tgfbr1* on myonuclear number
311 and signalling for protein synthesis as well as degradation. (A) No differences in myonuclear
312 lengths were observed in longitudinal sections of TA IIB myofibres of Acvr1b$^{fl/fl}$:Tgfbr1$^{fl/fl}$
313 compared to control animals. This indicates that simultaneous knockout of Acvr1b$^{fl/fl}$:Tgfbr1$^{fl/fl}$
314 did not affect the number of myonuclei per myofibre and that the myonuclear domain (i.e. cross-

315 sectional area/ nuclei (μm^2)) was almost doubled. Scale bar=100µm. (B) Western blot analysis
316 for Smad2/3 phosphorylation in TA and EDL muscle. (C) Relative gene expression of growth
317 factors in non-injured muscle. (D) Western blot analysis of phosphorylated and total Akt and
318 p70S6K in TA muscles. Results are presented as mean + SEM. N=5-8 mice. *: $P < 0.05$.
319 Significant difference between individual groups is indicated by lines with a *. Single *
320 indicates significant difference compared to all other groups at the same time point.

321 Myofibre specific receptor knockout affected the inflammatory response upon acute injury

322 After characterisation of uninjured TA muscles, effects of receptor knockout on early
323 TA muscle regeneration were examined two and four days after CTX acute injury. Two days
324 post injury, the injury site was characterised by increased interstitial space, indicating
325 degradation of the endomysium, and the presence of damaged myofibres, as can be observed
326 as unspecific green secondary antibody staining (Bencze, Periou, Baba-Amer, & Authier,
327 2019). Furthermore, mononuclear cells (i.e. inflammatory cells, fibroblasts or SCs) had
328 infiltrated the interstitial space within the injury site. Together, these observations indicate that
329 at 2 days post injury, the inflammatory response is high and damaged myofibres have not started
330 to regenerate yet. Four days post injury, the injury site was occupied by small, regenerating,
331 eMyHC^{+} myofibres with centrally located nuclei. Mononuclear cells were located in the
332 interstitial space, but the inflammatory response appears to be reduced compared to that
333 observed at 2 days post injury (Figure 4A). No significant differences in injury size between
334 groups were observed (Figure 4C).

335 Since various cell types in muscle tissue remain sensitive to TGF-β signalling in the
336 current model, effects of CTX injury on relative mRNA expression levels of *Tgfbr1, Acvr1b,*
337 *Tgf-β1* and *Mstn* were examined. Two and four days post injury, relative *Tgfbr1* expression was
338 increased in TA muscle of Tgfbr1$^{fl/fl}$ and Acvr1b$^{fl/fl}$:Tgfbr1$^{fl/fl}$ animals compared to day 0, which
339 suggests that *Tgfbr1* mRNA is highly expressed in mononuclear cells (i.e. fibroblasts,
340 inflammation cells and SCs) that infiltrate the injury site. For all groups, relative *Tgf-β1*
341 expression peaked at day 2 post injury. At day 4 post injury in Acvr1b$^{fl/fl}$:Tgfbr1$^{fl/fl}$ animals,
342 *Tgf-β1* expression levels remained significantly increased compared to those of other groups
343 (Figure 4D).

344 At day 2 and 4, *Acvr1b* expression in Tgfbr1$^{fl/fl}$ and control animals decreased compared
345 to day 0, whereas *Acvr1b* expression in Acvr1b$^{fl/fl}$ and Acvr1b$^{fl/fl}$:Tgfbr1$^{fl/fl}$ animals increased.

346 Relative *Mstn* expression levels were decreased at day 2 and 4 post injury. These data suggest
347 that under control conditions *Acvr1b* and *Mstn* are highly expressed in skeletal myofibres, while
348 mononuclear cells that infiltrate the injury site express relatively little *Acvr1b* and *Mstn* (Figure
349 4D).

350 TGF-β1 plays an important role in the early inflammatory response after acute muscle
351 injury. Inflammatory cells (i.e. neutrophils and macrophages), which infiltrate damaged muscle,
352 digest cellular debris and secrete inflammatory cytokines, such as interleukin-1β (*Il-1β*) and *Il-*
353 *6*. Here, we showed that in all groups, relative mRNA levels of macrophage specific protein
354 cluster of differentiation 68 (*Cd68*) (da Silva, Platt, de Villiers, & Gordon, 1996; M. J. Smith
355 & Koch, 1987), *Il-1β* and *Il-6* peaked two days post injury. At day 0 and 4, in TA muscle of
356 Acvr1b$^{fl/fl}$:Tgfbr1$^{fl/fl}$ animals *Cd68* expression was increased compared to all other groups or
357 control animals, respectively. At day 0 and 4, macrophage specific *Cd163* (Schaer et al., 2001)
358 expression levels of Acvr1b$^{fl/fl}$:Tgfbr1$^{fl/fl}$ animals were increased compared to those of
359 Acvr1b$^{fl/fl}$ or Tgfbr1$^{fl/fl}$ animals (Figure 4D). At day 0 in Acvr1b$^{fl/fl}$:Tgfbr1$^{fl/fl}$ animals
360 expression levels of *Il-1β* were increased compared to those of Acvr1b$^{fl/fl}$ and Tgfbr1$^{fl/fl}$ animals.
361 Upon injury, no differences in *Il-1β* and *Il-6* expression levels were observed between groups
362 (Figure 4D). Together, these results suggest that in this model the inflammatory response peaks
363 approximately 2 days post injury.

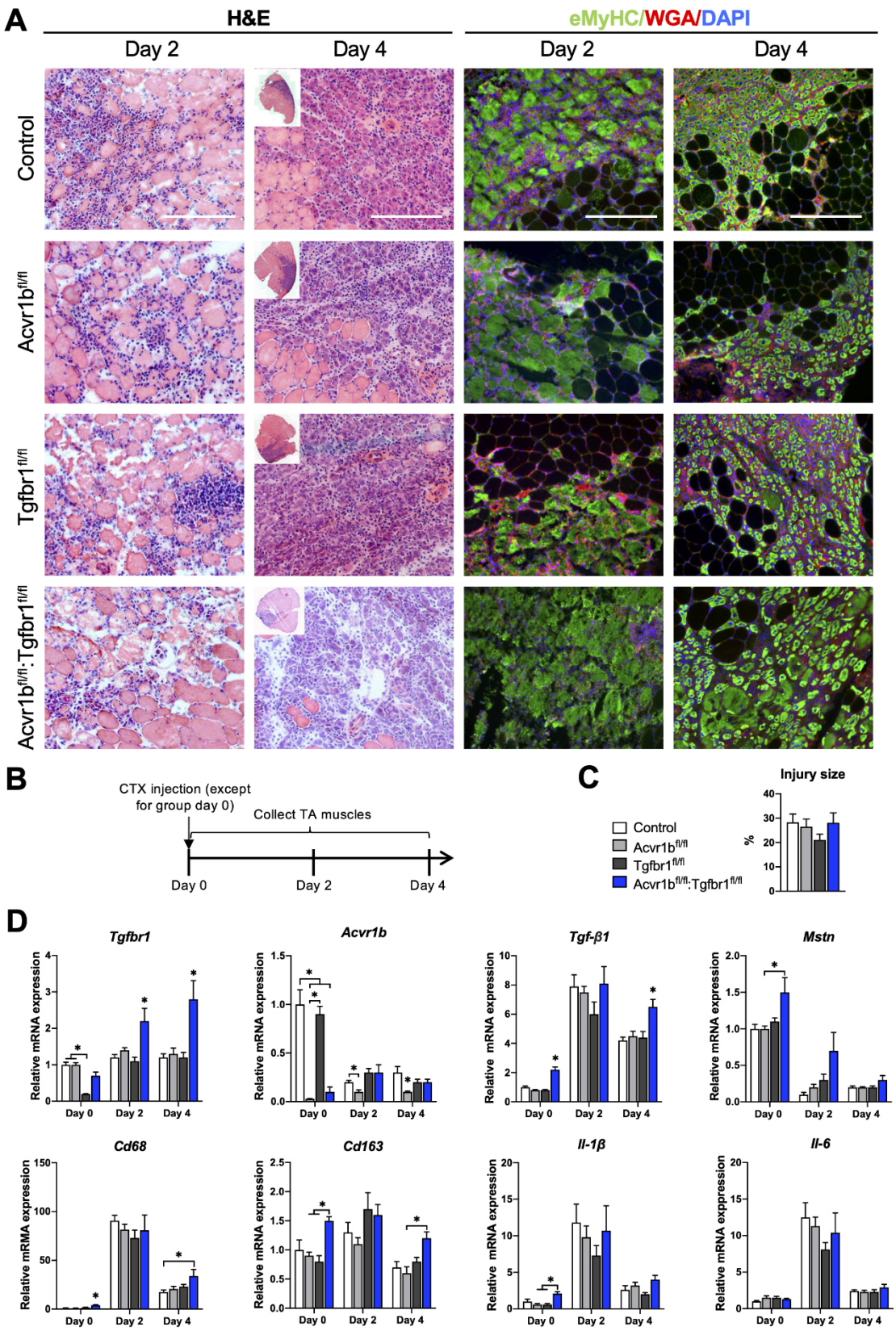

364

365 **Figure 4.** Immune response was slightly enhanced in muscle of Acvr1b$^{fl/fl}$:Tgfbr1$^{fl/fl}$ mice. (A)

366 Representative images of H&E and eMyHC staining of TA sections at 2 and 4 days after CTX

367 injection. Scale bars=250 μm. (B) Scheme shows CTX injection in TA and sample collection.
368 (C) Percentage of injury area was not significantly different between groups. (D) Relative gene
369 expressions in TA in the absence (day 0) or presence of CTX injection after 2 and 4 days.
370 Results are presented as mean + SEM. N=5-8 mice, *: $P < 0.05$. Significant difference between
371 individual groups is indicated by lines with a *. Single * indicates significant difference
372 compared to all other groups at the same time point.
373
374 Lack of both *Acvr1b* and *Tgfbr1* stimulated CSA of regenerating myofibres, myogenic gene
375 expression and number of differentiating muscle cells during regeneration
376 Effects of receptor knockout on muscle regeneration after acute injury were examined
377 (Figure 5A). In Acvr1b$^{fl/fl}$:Tgfbr1$^{fl/fl}$ animals CSA of regenerating myofibres was increased
378 compared to Acvr1b$^{fl/fl}$ and Tgfbr1^{flfl} animals, but not compared to controls (Figure 5B).
379 Regeneration index (RI) was reduced in muscle tissue of Acvr1b$^{fl/fl}$ and Tgfbr1^{flfl} animals
380 compared to that of control animals, while RI of Acvr1b$^{fl/fl}$:Tgfbr1$^{fl/fl}$ animals was not
381 significantly different compared to that of other three groups (Figure 5B). Next, we
382 hypothesized an increased immune response was involved in the accelerated muscle
383 regeneration process after cardiotoxin induced muscle injury in the absence of Acvr1b and
384 Tgfbr1. Macrophages were identified by F4/80 in IF staining (Figure 5-figure supplement 1).
385 The number of macrophages in TA of Acvr1b$^{fl/fl}$:Tgfbr1$^{fl/fl}$ animals at day 4 post injury was
386 significantly increased compared to that in control animals (Figure 5C). Taken together, after
387 acute injury individual knockout of *Acvr1b* or *Tgfbr1* expression in mature myofibre reduced
388 myofibre regeneration, while simultaneous knockout of *Acvr1b* and *Tgfbr1* stimulated this
389 which was accompanied by increased infiltration of macrophages.
390 The effects of receptor knockout on expression of genes involved in SC activation,
391 differentiation and muscle growth were analysed in order to understand observed differences in

392 RI and CSA of regenerating myofibres. First of all, mRNA expression levels of various growth
393 factors were differently affected by receptor knockout. *Hgf* and *Mgf* expression peaked at day
394 2 post injury. At day 2 in Acvr1b$^{fl/fl}$ and Acvr1b$^{fl/fl}$:Tgfbr1$^{fl/fl}$ mice *Mgf* expression was lower
395 compared to control animals. At day 4 in Acvr1b$^{fl/fl}$:Tgfbr1$^{fl/fl}$ animals *Igf1ea* levels were
396 increased compared to those of Acvr1b$^{fl/fl}$ and control animals. *Vegf* and *Fgf-2* expression levels
397 decreased after injury. At day 2 in Acvr1b$^{fl/fl}$:Tgfbr1$^{fl/fl}$ mice *Fgf-2* expression was increased
398 (Figure 5D). Together, these results indicate that in simultaneous receptor knockout enhanced
399 *Igf1ea* and *Fgf-2* expression post injury contribute to the accelerated early regeneration.
400 Proper muscle regeneration is regulated by sequential expression of myogenic genes.
401 Thus, relative mRNA expression levels of myogenic genes (i.e., paired box protein 7 (*Pax7*),
402 myoblast determination protein 1 (*Myod*), myogenin (*Myog*), muscle embryonic myosin heavy
403 chain (*Myh3*) as well as inhibitor of differentiation 1 (*Id1*)), were examined. At day 4, in all
404 groups expression of *Pax7, Myod, Myog* and *Myh3* had increased. At day 0 in
405 Acvr1b$^{fl/fl}$:Tgfbr1$^{fl/fl}$ mice, *Pax7* expression was increased compared to that of Tgfbr1$^{fl/fl}$ mice,
406 while at day 4 in Acvr1b$^{fl/fl}$:Tgfbr1$^{fl/fl}$ mice *Pax7* expression was increased compared to that in
407 all other groups. At day 0 in Acvr1b$^{fl/fl}$:Tgfbr1$^{fl/fl}$ mice *Myod* and *Myog* expression levels were
408 increased compared to those in other groups, while at day 2 in Acvr1b$^{fl/fl}$:Tgfbr1$^{fl/fl}$ mice *Myod*
409 expression levels were increased compared to those in Tgfbr1$^{fl/fl}$ mice and *Myog* expression
410 levels were increased compared to those in both Acvr1b$^{fl/fl}$ and Tgfbr1$^{fl/fl}$ animals. At day 4 post
411 injury, no differences in *Myod* or *Myog* expression levels were observed between groups,
412 although a trend suggested that expression of both genes was increased in Acvr1b$^{fl/fl}$:Tgfbr1$^{fl/fl}$
413 mice. At both day 0 and day 2, in Acvr1b$^{fl/fl}$:Tgfbr1$^{fl/fl}$ mice *Myh3* levels were increased
414 compared to those in both Acvr1b$^{fl/fl}$ and control animals. At day 4 post injury, no differences
415 in *Myh3* expression were observed between groups (Figure 5D). Receptor knockout did not

416 affect *Id1* expression. Taken together, these results show that in TA myofibre specific *Acvr1b*
417 and *Tgfbr1* receptor knockout stimulates myogenic gene expression.
418 Lastly, relative expression levels of muscle specific E3 ligases MuRF-1 and atrogin-1
419 during early regeneration were considered. MuRF-1 and atrogin-1 are expressed in mature
420 myofibres, but not in SCs and inhibit myofibre growth and hypertrophy. For Acvr1b$^{fl/fl}$,
421 Tgfbr1$^{fl/fl}$ and control animals, at day 4 *Murf-1* levels were decreased compared to those at day
422 0, while for Acvr1b$^{fl/fl}$:Tgfbr1$^{fl/fl}$ animals no significant differences in *Murf-1* expression were
423 observed over time. At both day 2 and 4 post injury, in Acvr1b$^{fl/fl}$:Tgfbr1$^{fl/fl}$ animals *Atrogin-1*
424 expression levels were relatively increased compared to those in Acvr1b$^{fl/fl}$ mice, while no
425 differences in *Murf-1* expression levels were observed between groups (Figure 5D). Together,
426 these results indicate E3 ligases do not play a role in the observed increase in size of
427 regenerating myofibres.
428 On day 0, the number of proliferating cells (Ki67^{+}) in low oxidative region of TA of
429 Acvr1b$^{fl/fl}$:Tgfbr1$^{fl/fl}$ animals was about 7.6-fold higher than that in control animals (Figure 5E).
430 Two days after injury, a 6-fold increase of proliferating cells was found in Acvr1b$^{fl/fl}$:Tgfbr1$^{fl/fl}$
431 animals compared to that on day 0. Moreover, at day 4 after injury, the number of proliferating
432 cells in Acvr1b$^{fl/fl}$:Tgfbr1$^{fl/fl}$ animals was 1.7-fold higher than that in control animals. To
433 determine whether the increased CSA of regenerating myofibres in Acvr1b$^{fl/fl}$:Tgfbr1$^{fl/fl}$
434 animals was due to an increased SCs number and advanced differentiation of myoblasts, we
435 tested SCs proliferation and activation status. Although at day 0 and 4, the number of SCs
436 (Pax7^{+}) cells was more in Acvr1b$^{fl/fl}$:Tgfbr1$^{fl/fl}$ animals compared to that in control animals
437 (Figure 5F), the number of proliferating SCs (Ki67^{+}/Pax7^{+}) did not differ from that in control
438 (Figure 5G, Figure 5-figure supplement 2,). Nevertheless, an accelerated rate of increase in
439 Ki67^{+}/Pax7^{+} cells was shown. Note that, at day 4 after injury the number of myogenin^{+} cells
440 was more than 2.2-fold higher in Acvr1b$^{fl/fl}$:Tgfbr1$^{fl/fl}$ animals (Figure 5H, Figure 5-figure

441 supplement 3). These findings indicate that muscle regeneration upon acute injury was
442 improved in Acvr1b$^{fl/fl}$:Tgfbr1$^{fl/fl}$ animals, which was attributed to an accelerated myogenic
443 process.

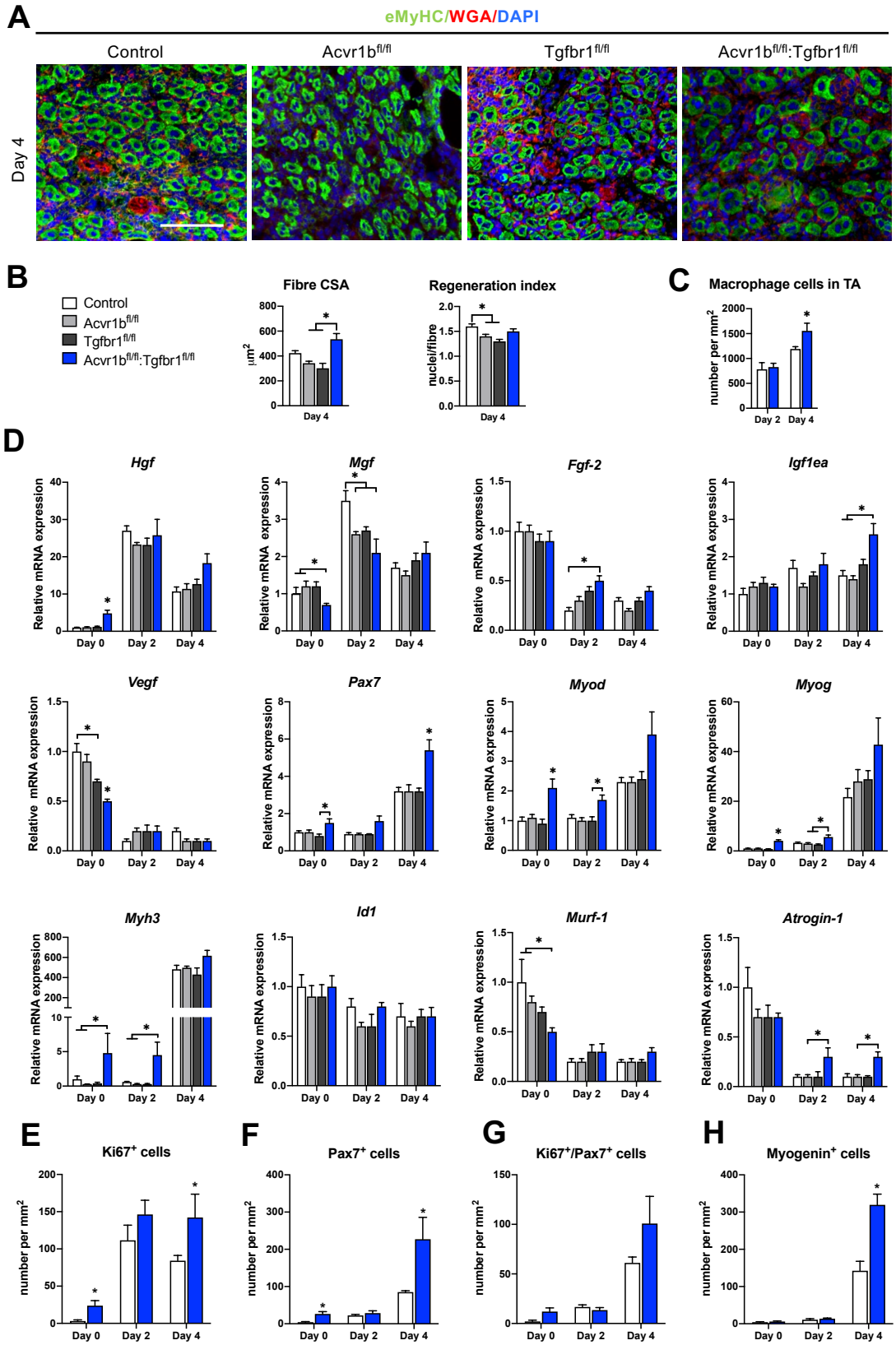

Figure 5. Acvr1b$^{fl/fl}$:Tgfbr1$^{fl/fl}$ mice showed enhanced CSA of regenerating myofibres and early enhanced expression of myogenic genes and differentiating cells after acute injury. (A) IF

447 staining images represent eMyHC^{+} myofibres 4 days after CTX injection. Scale bar=100µm.
448 (B) CSA of eMyHC^{+} myofibres in injured area increased in Acvr1b$^{fl/fl}$:Tgfbr1$^{fl/fl}$ mice compared
449 to Acvr1b$^{fl/fl}$ and Tgfbr1$^{fl/fl}$ animals, while RI was decreased in both Acvr1b$^{fl/fl}$ and Tgfbr1$^{fl/fl}$
450 mice compared to controls. (C) Number of macrophages was quantified in the injured area. (D)
451 Relative gene expression in TA in absence (day 0) or presence of CTX injection after 2 and 4
452 days are presented. Increased number of Ki67^{+} cells (E) and Pax7^{+} (F) cells were found in TA
453 of Acvr1b$^{fl/fl}$:Tgfbr1$^{fl/fl}$ mice in absence of injury as well as 4 days after CTX injection. (G) Four
454 days post injury, number of Ki67^{+}/Pax7^{+}cells was not different between control and
455 Acvr1b$^{fl/fl}$:Tgfbr1$^{fl/fl}$ mice. (H) More Myogenin^{+} cells were found in injured area of
456 Acvr1b$^{fl/fl}$:Tgfbr1$^{fl/fl}$ mice on day 4 post injury. Results are presented as mean + SEM. N=5-8
457 mice, *: $P < 0.05$. Significant difference between individual groups is indicated by lines with a
458 *. Single * indicates significant difference compared to all other groups at the same time point.
459

460 Simultaneous knockout of both *Acvr1b* and *Tgfbr1* within the myofibre enhanced ECM
461 deposition

462 Another essential aspect of muscle regeneration is connective tissue remodelling. Figure 5A
463 shows Sirius Red stainings at different stages of regeneration. At day 0, myofibres were
464 surrounded by a thin layer of endomysium. At 2 days post injury, this endomysium appears to
465 be disrupted for a large part. At day 4 post injury, a large amount of connective tissue may be
466 observed surrounding the regenerating myofibres (Figure 6A).

467 Effects of myofibre specific *Acvr1b* and *Tgfbr1* receptor knockout on ECM remodelling
468 were assessed by examining connective tissue growth factor (*Ctgf*), collagen type 1, alpha 1
469 (*Col1a1*) and collagen type 3, alpha 1 (*Col3a1*) expression. At all times, in Acvr1b$^{fl/fl}$:Tgfbr1$^{fl/fl}$
470 animals *Ctgf* and *Col1a1* mRNA expression levels were substantially increased compared to
471 those of control animals or all groups. At day 0, in Acvr1b$^{fl/fl}$:Tgfbr1$^{fl/fl}$ animals, *Col3a1*

472 expression levels were increased compared to those in other groups. At day 2 and 4, in
473 Acvr1b$^{fl/fl}$:Tgfbr1$^{fl/fl}$ animals *Col3a1* expression was increased compared to Acvr1b$^{fl/fl}$ or both
474 Acvr1b$^{fl/fl}$ and Tgfbr1$^{fl/fl}$ animals (Figure 6B).

475 To determine whether the number of fibroblasts was increased in TA muscles by
476 knockout of *Acvr1b* and *Tgfbr1*, we assessed relative mRNA expression levels of fibroblast
477 markers, transcription factor 4 (*Tcf4*) and platelet-derived growth factor receptor A (*Pdgfra*)
478 (Mathew et al., 2011), were determined. At day 0, *Tcf4* expression levels of TA in Acvr1b$^{fl/fl}$
479 mice were increased compared to those in control animals, but were not different from those in
480 Tgfbr1$^{fl/fl}$ or Acvr1b$^{fl/fl}$:Tgfbr1$^{fl/fl}$ animals. In Acvr1b$^{fl/fl}$:Tgfbr1$^{fl/fl}$ animals, relative *Pdgfra*
481 expression levels were increased compared to those of control and Acvr1b$^{fl/fl}$ animals.
482 Noteworthy, four days post injury, both *Tcf4* and *Pdgfra* mRNA levels were increased in
483 Acvr1b$^{fl/fl}$:Tgfbr1$^{fl/fl}$ animal compared to those in control mice (Figure 6C).

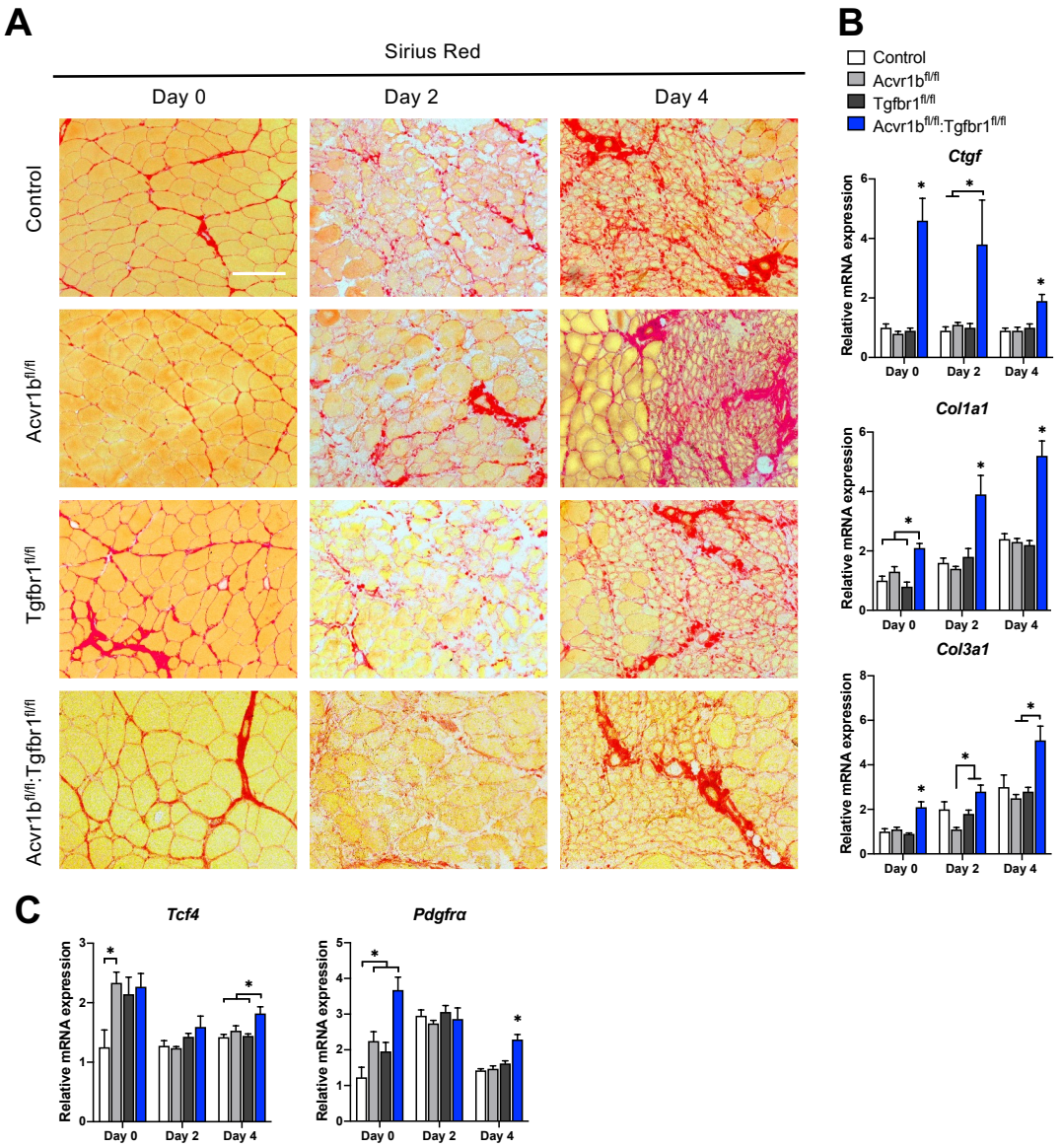

484

485 **Figure 6.** Relative mRNA expression levels of ECM components were enhanced in

486 Acvr1b$^{fl/fl}$:Tgfbr1$^{fl/fl}$ mice. (A) Sirius Red staining shows collagen deposition in absence (day

487 0) or presence of CTX injection after 2, and 4 days (scale bar=100μm). (B, C) Relative gene
488 expression in TA muscle in absence (day 0) or presence of CTX injection after 2 and 4 days.
489 Results are presented as mean + SEM. N=5-8 mice, *: $P < 0.05$. Significant difference between
490 individual groups is indicated by lines with a *. Single * indicates significant difference
491 compared to all other groups at the same time point.

492 **Discussion**

493 The aim of this study was to investigate effects of mature myofibre specific knockout of type I
494 receptors *Tgfbr1* and *Acvr1b* on muscle morphology as well as early muscle regeneration,
495 inflammation and collagen deposition in both uninjured muscle tissue and after acute CTX
496 injury. We observed that simultaneous knockout of *Acvr1b* and *Tgfbr1* resulted in a substantial
497 increase in TA and EDL muscle mass as well as type IIB myofibre CSA. *Tgfbr1* knockout only
498 marginally increased muscle mass, while *Acvr1b* knockout did not affect muscle mass. In the
499 low oxidative region of TA muscle tissue of Acvr1b$^{fl/fl}$:Tgfbr1$^{fl/fl}$ animals the percentage of type
500 IIB myofibres was reduced, while in EDL no differences in myofibre type distribution were
501 observed. Remarkably, simultaneous knockout of both *Acvr1b* and *Tgfbr1* caused spontaneous
502 regeneration and an increase in SC number in the low oxidative region of TA and in EDL
503 muscle tissue. Lack of both *Acvr1b* and *Tgfbr1* in the skeletal myofibre of TA increased
504 myofibre CSA of regenerating myofibres, number of regenerating cells and macrophages
505 during regeneration, as well as enhanced expression levels of myogenic gene expression and
506 growth factors. In both uninjured and regenerating muscles, simultaneous knockout of *Acvr1b*
507 and *Tgfbr1* in the myofibre resulted in increased ECM and fibroblasts gene expression. Figure
508 7 shows a schematic summarising the main results.

509 Together, these results indicate that simultaneous receptor knockout stimulates muscle
510 hypertrophy and promotes early muscle regeneration upon injury, whereas individual receptor
511 knockout does not.

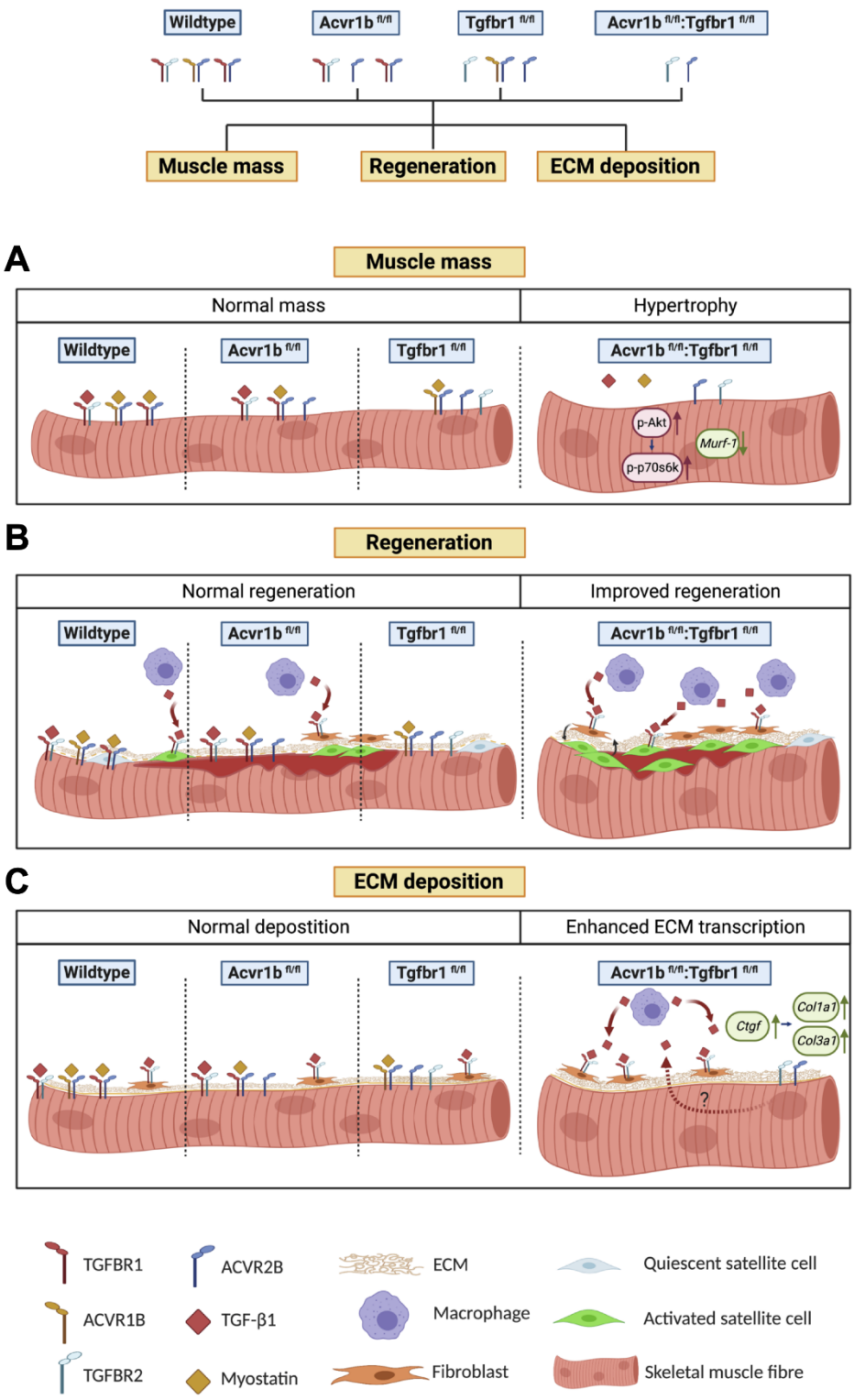

512

513 **Figure 7.** Schematic diagram of the effects of single or combined muscle specific knockout of

514 *Tgfbr1* and/or *Acvr1b* receptors on muscle hypertrophy, regeneration and expression of ECM

515 components. (A) Myofibre size is not affected after individual knockout of *Acvr1b* or *Tgfbr1*,

516 which indicates that these receptors have redundant effects on muscle size and that myostatin
517 signals via both receptors to control muscle mass. Simultaneous knockout of both *Acvr1b* and
518 *Tgfbr1* inhibits signalling of TGF-β, myostatin and activin A and stimulates protein synthesis
519 via the Akt/mTOR/p70S6K pathway, while inhibiting protein breakdown through repression of
520 *Murf-1* levels, resulting in substantial muscle hypertrophy. (B) Upon acute injury, simultaneous
521 knockout of combined *Acvr1b* and *Tgfbr1* accelerates early muscle regeneration, as observed
522 by increased myogenic gene expression as well as increased CSA of regenerating myofibres.
523 An increased number of SCs likely contributes to these effects. (C) Simultaneous myofibre
524 specific knockout of *Acvr1b* and *Tgfbr1* induces mRNA expression of ECM components. These
525 effects are likely caused by enhanced TGF- β1 signalling in fibroblasts. Schematic is created
526 using BioRender.
527
528 <u>Simultaneous knockout of *Acvr1b* and *Tgfbr1* induces hypertrophy by both inhibiting protein</u>
529 <u>degradation and stimulating protein synthesis</u>
530 Our data show that simultaneous myofibre specific knockdown of both *Acvr1b* and *Tgfbr1* is
531 required for muscle hypertrophy, while inhibition of *Acvr1b* does not affect muscle mass or
532 myofibre size and inhibition of *Tgfbr1* has only marginal effects. Supporting our data, a recent
533 study showed that simultaneous inhibition of *Acvr1b* and *Tgfbr1* was required to enhance
534 muscle mass, while individual receptor inhibition had little effect (Lee et al., 2020). These
535 results indicate that *Acvr1b* and *Tgfbr1* have redundant functions in the regulation of muscle
536 mass.
537 Myostatin and activin A negatively regulate muscle mass by stimulating protein
538 degradation through upregulation of E3 ligases and reducing protein synthesis through a
539 decrease in phosphorylation of Akt and its downstream target p70S6K (Amirouche et al., 2009;
540 J. L. Chen et al., 2014; McFarlane et al., 2006; Trendelenburg et al., 2009). TGF-β

541 overexpression *in vivo* has been suggested to increase atrogin-1 expression and concomitantly
542 cause muscle atrophy (Mendias et al., 2012). Simultaneous receptor knockout increased relative
543 expression of phosphorylated Akt and lack of both *Acvr1b* and *Tgfbr1* increased the
544 phosphorylated p70S6K/total p70S6K ratio, which indicates increased protein synthesis via the
545 Akt/mTOR/p70S6K pathway contributes to muscle hypertrophy.

546 Simultaneous knockout of *Acvr1b* and *Tgfbr1* also reduced mRNA expression levels of
547 E3 ligases *Murf-1*, indicating reduced protein degradation. Simultaneous knockout of *Acvr1b*
548 and *Tgfbr1* increased *Hgf* expression levels. HGF signalling has been shown to protect skeletal
549 muscle against atrophy after denervation or in muscle pathology by reducing relative *Murf-1*
550 and *Atrogin-1* expression levels (Choi, Lee, Lee, Ko, & Kim, 2018). Together, these results
551 indicate that simultaneous knockout of both *Acvr1b* and *Tgfbr1* both decrease protein
552 breakdown and stimulate protein synthesis.

553 The TGF-β type I receptor knockout induced an increase in Akt signalling and reduction
554 in E3 ligase expression are likely mediated at least in part via elevated *Hgf* expression levels in
555 myofibres. In both myoblasts and myotubes, HGF stimulates the Akt/mTOR pathway (A. L.
556 Chen et al., 2012; Perdomo et al., 2008). In addition, reduced Smad2/3 phosphorylation within
557 myofibres likely contributes to the increase in Akt signalling and reduction in E3 ligase
558 expression (Goodman, McNally, Hoffmann, & Hornberger, 2013; Sartori et al., 2009). In TA
559 and EDL of Acvr1b$^{fl/fl}$:Tgfbr1$^{fl/fl}$ animals, Smad2/3 phosphorylation was or tended to be
560 reduced, respectively. Note that TGF-β type I receptors were specifically knocked out in
561 myofibres and that Smad2/3 in various other cell types can still be phosphorylated by TGF-β1,
562 myostatin and activin A, masking the changes in myofibres.

563 TGF-β1, myostatin and activin A regulate skeletal muscle mass via similar mechanisms.
564 Previous research has shown that inhibition of myostatin and to a lesser extent activin A is
565 sufficient to induce muscle hypertrophy (Wu et al., 2017). Here we show that inhibition of

566 TGF-β1 or activin A signalling via their type I receptor is insufficient to induce muscle
567 hypertrophy. In muscle myostatin likely signals via both type I receptors to regulate muscle
568 mass. In muscles that lack either *Acvr1b* or *Tgfbr1,* we observed no changes in Smad2/3
569 signalling, which is in accordance with the observation there is no or modest effect on muscle
570 hypertrophy. Targeting both receptors is indispensable to substantially reduce TGF-
571 β1/myostatin/activin A signalling and induce muscle hypertrophy.
572
573 Simultaneous knockout of *Acvr1b* and *Tgfbr1* specifically enhances type IIB myofibre CSA
574 without accretion of myoblasts
575 Simultaneous knockout of *Acvr1b* and *Tgfbr1* most substantially increased type IIB myofibre
576 CSA. This is likely the result of myofibre type-related hypertrophic capacity rather than
577 myofibre type-specific receptor knockout bias (McCarthy et al., 2012b). It has been suggested
578 that mainly fast twitch myofibres possess the ability to hypertrophy, while slow twitch
579 myofibres are unlikely to increase in size (van Wessel et al., 2010). Additionally, ACVR2B is
580 more abundantly expressed in type II than type I myofibres, thus a more substantial effect on
581 myofibre hypertrophy was expected upon type I receptor depletion (Babcock, Knoblauch, &
582 Clarke, 2015). Remarkably, type IIB myofibre hypertrophy occurred without apparent accretion
583 of myonuclei, which resulted in an approximately 70% increase in myonuclear domain. The
584 lack of difference in the number of myonuclei per myofibre cross-section together with the lack
585 of difference in myonuclear length in type IIB myofibres of TA indicates that the total number
586 of nuclei per myofibre was not affected by simultaneous knockout of *Acvr1b* and *Tgfbr1*.
587 Although e.g. exercise induced hypertrophy is often accompanied by increased myonuclei
588 number (Conceicao et al., 2018; van der Meer, Jaspers, Jones, & Degens, 2011), the myonuclear
589 domain is known to be flexible and increases in myonuclear domain of 30% have been reported
590 (Murach, Englund, Dupont-Versteegden, McCarthy, & Peterson, 2018). Moreover, inhibition

591 of myostatin signalling using soluble ACVR2B leads to hypertrophy without accretion of SCs
592 (Lee et al., 2012). Here, we show that in type IIB myofibres myonuclear domain can increase
593 by at least 70%, without requirement of accretion of myonuclei to sustain myofibre growth. To
594 the best of our knowledge such increase in myonuclear domain has not been reported before.

595 Since myonuclei are required for mitochondrial biogenesis, a local reduction in
596 oxidative capacity was expected (Hock & Kralli, 2009; Kotiadis, Duchen, & Osellame, 2014).
597 In this study, knockout of both *Acvr1b* and *Tgfbr1* resulted in decreased SDH activity in the
598 low oxidative region of TA. Previous research has shown that an inverse relation exists between
599 myofibre CSA and oxidative capacity, whereas myofibre CSA is positively correlated to
600 glycolytic capacity (Rivero, Talmadge, & Edgerton, 1998). Recent evidence suggests that,
601 similar to "Warburg effect" in tumours, in hypertrophying skeletal muscle reprogramming
602 towards a more glycolytic metabolism occurs. Glycolytic enzyme pyruvate kinase muscle
603 isoform 2 (PKM2), which is particularly highly expressed in type II myofibres, contributes to
604 the increased hypertrophic potential of type II myofibres (Verbrugge et al., 2020).

605 Although lack of *Acvr1b* and *Tgfbr1* decreased SDH activity, integrated SDH activity
606 (SDH activity times CSA) was increased. Previous research has shown that integrated SDH
607 activity correlates with the maximal rate of oxygen consumption (VO_{2max}) and mitochondrial
608 density, which suggests that the total oxidative capacity of these myofibres in
609 $Acvr1b^{fl/fl}$:$Tgfbr1^{fl/fl}$ animals was increased (W. J. van der Laarse, Diegenbach, & Elzinga,
610 1989). Present data show that by targeting both receptors simultaneously it is possible to deviate
611 from the tight relation between myofibre size and oxidative metabolism (i.e. simultaneous
612 increases in both myofibre size and oxidative capacity). The role of both receptors in the
613 synthesis of mitochondria warrants further investigation.

614

615 Lack of both *Acvr1b* and *Tgfbr1* reduces the percentage of type IIB myofibres within the low
616 oxidative region of the TA
617 Another remarkable finding was the reduction in the percentage of type IIB myofibres in the
618 low oxidative region of the TA muscle of Acvr1b$^{fl/fl}$:Tgfbr1$^{fl/fl}$ animals. In the high oxidative
619 region of the TA muscle as well as the EDL, no differences in myofibre type distribution were
620 observed. In contrast to our findings, previous research has shown increased percentage of fast,
621 glycolytic myofibres in skeletal muscle of Mstn$^{-/-}$ mice (Amthor et al., 2007; Girgenrath, Song,
622 & Whittemore, 2005; Hennebry et al., 2009). Moreover, increased myostatin/activin A
623 signalling in follistatin mutant mice showed increased the percentage of slow, oxidative
624 myofibres (Lee et al., 2010). Note that in a genetic knockout mouse model, absence of
625 myostatin precedes myogenesis and may influence skeletal muscle development, whereas in
626 our model TGF-β signalling was inhibited in mature skeletal muscle. The reduction in type IIB
627 myofibres may also be a consequence of local damage to the myofibres, rather than a
628 phenotypical change caused by receptor knockout. Taken together, these results indicate type I
629 receptor knockout in mature myofibres has minor effects on myofibre type distribution.
630
631 Simultaneous knockout of *Acvr1b* and *Tgfbr1* in myofibre may result in accelerated early
632 regeneration
633 We observed that simultaneous knockout of *Acvr1b* or *Tgfbr1* increased the CSA of
634 regenerating myofibres compared to individual receptor knockout, while a trend was visible
635 compared to controls. In addition, at day 0, simultaneous receptor knockout enhanced *Hgf*
636 expression as well as the number of SCs per myofibre and concomitantly relative expression
637 levels of *Pax7* and *Myod,* indicating that SCs were activated prior to CTX injection. Muscle
638 regeneration is dependent on activation of Pax7^{+} SCs and sequential expression of myogenic
639 genes (Charge & Rudnicki, 2004; Delaney, Kasprzycka, Ciemerych, & Zimowska, 2017; Ishido

640 & Kasuga, 2011; Lepper, Partridge, & Fan, 2011). HGF is the primary growth factor for SC
641 activation and may have accelerated early muscle regeneration (Allen, Sheehan, Taylor,
642 Kendall, & Rice, 1995; Gal-Levi, Leshem, Aoki, Nakamura, & Halevy, 1998; Miller, Thaloor,
643 Matteson, & Pavlath, 2000; Tatsumi et al., 1998). Receptor knockout did not affect *Hgf*
644 expression after injury, which indicates HGF expression and subsequent SC activation is likely
645 not induced by lack of TGF-β signalling in the myofibre, but rather a consequence of
646 spontaneous damage and regeneration.

647 Moreover, 2 or 4 days post injury simultaneous knockout of *Acvr1b* and *Tgfbr1*
648 increased expression levels of *Fgf-2* or *Igf1ea*. Simultaneous overexpression of IGF-1 and FGF-
649 2 has a synergistic effect on both myoblast proliferation as well as fusion index (Allen &
650 Boxhorn, 1989). Thus, simultaneous knockout of *Acvr1b* and *Tgfbr1* in skeletal myofibre likely
651 enhances early muscle regeneration via enhanced expression of *Igf1ea* and *Fgf-2.* However,
652 myogenic gene expression was increased prior to *Igf1ea* and *Fgf-2* upregulation, which
653 indicates that although these growth factors may positively contribute to early regeneration,
654 upregulation of *Igf1ea* and *Fgf-2* cannot fully explain effects on early regeneration.

655 Simultaneous receptor knockout did not reduce mRNA expression of E3 ligases during
656 regeneration, indicating that the increase in myofibre CSA is not caused by reduced protein
657 breakdown. In contrast, during regeneration *Atrogin-1* expression is enhanced in
658 Acvr1b$^{fl/fl}$:Tgfbr1$^{fl/fl}$ animals compared to other groups, but here the enhanced *Atrogin-1* levels
659 may correspond with muscle regeneration.

660 Moreover, for Acvr1b$^{fl/fl}$:Tgfbr1$^{fl/fl}$ animals the numbers of SCs and differentiating
661 myoblasts within the injured regions 4 days post injury were more than doubled compared to
662 those in control animals. The observation that at all time points the number of proliferating SCs
663 (i.e. Ki67^{+}/Pax7^{+} cells) was not different between control and Acvr1b$^{fl/fl}$:Tgfbr1$^{fl/fl}$ animals
664 indicates that in the Acvr1b$^{fl/fl}$:Tgfbr1$^{fl/fl}$ animals muscle damage had initiated activation and

665 proliferation in the injured region between day 2 and 4. Alternatively, SCs had migrated from
666 adjacent myofibres to the site of injury or from intact regions along the myofibres (Ishido &
667 Kasuga, 2011; Schultz, Jaryszak, & Valliere, 1985). The accelerated myoblast proliferation and
668 differentiation likely contributed to the enhanced protein synthesis and hypertrophy of newly
669 formed myofibres.

670 A limitation of this study is that we did not observe later stages of muscle regeneration.
671 Additional research is required to determine whether changes observed in this study ultimately
672 result in a shorter regeneration period.

673

674 *Acvr1b* and *Tgfbr1* affect inflammatory response after injury

675 Proper activation of the immune response and expression of inflammatory cytokines is
676 important for myoblast proliferation and myogenic gene expression during early muscle
677 regeneration (Cantini et al., 1995; Chaweewannakorn et al., 2018; Grabiec et al., 2013; Zhang
678 et al., 2013). In absence of injury, compared with control, 8912310-fold more number of
679 macrophages was found the in low oxidative area of TA in Acvr1b$^{fl/fl}$:Tgfbr1$^{fl/fl}$ animals,
680 indicating increased immune cells residence at baseline before CTX injury. Two days post
681 injury a large infiltration of mononucleated cells was observed in all groups, as well as a peak
682 in relative expression levels of *Tgf-β1*, *Cd68*, *Il-1β* and *Il-6*.

683 Macrophages play an important role in regulation of muscle regeneration (Tidball,
684 2017). Macrophages are classified in M1 (pro-inflammatory) and M2 (anti-inflammatory)
685 macrophages (Mosser & Edwards, 2008). Early after injury, gene expression of pan-
686 macrophages marker *Cd68* and M2 macrophage marker *Cd163* (Hu et al., 2017), as well as the
687 number of macrophages were increased in both control and Acvr1b$^{fl/fl}$:Tgfbr1$^{fl/fl}$ animals.
688 Expression levels *Il-6* and *Il-1β*, which are typical cytokines expressed by M1 macrophages,
689 were not higher than in control animals, while *Igf-1ea* expression, also known to be expressed

690 by M1 macrophages, was increased in Acvr1b$^{fl/fl}$:Tgfbr1$^{fl/fl}$ animals which was likely
691 advantageous to expand the SC pool and to induce hypertrophy of newly formed myofibres.
692 Moreover, TGF-β1 expression was increased in muscle with simultaneous knockout of
693 Acvr1b$^{fl/fl}$:Tgfbr1$^{fl/fl}$. At a later stage after injury, M2 macrophages are known to promote
694 myogenic differentiation and stimulate ECM deposition by releasing TGF-β1 (Arnold et al.,
695 2007; Novak, Weinheimer-Haus, & Koh, 2014). Taken together, we conclude that muscle-
696 specific lack of both receptors promotes an inflammatory response by enhanced infiltration of
697 macrophages which is associated with accelerated muscle regeneration.
698

699 Lack of both *Acvr1b* and *Tgfbr1* enhances gene expression of ECM components in both intact
700 and injured TA muscle

701 In both uninjured TA muscle tissue, as well as after CTX injury simultaneous knockout of
702 *Tgfbr1* and *Acvr1b* in skeletal myofibre increased *Ctgf*, *Col1a1* and *Col3a1* mRNA expression.
703 These increases in gene expression were conceivably caused by TGF-β signalling in other cell
704 types present within the muscle tissue, i.e. fibroblasts. This hypothesis is supported by the
705 infiltration of fibroblasts in TA muscle of Acvr1b$^{fl/fl}$:Tgfbr1$^{fl/fl}$ animals in the absence of injury,
706 as well as increased gene expression levels of *Pdgfrα*. Furthermore, after injury in
707 Acvr1b$^{fl/fl}$:Tgfbr1$^{fl/fl}$ animals *Tgfbr1, Tcf4* and *Pdgfrα* levels were increased compared to those
708 in groups, which indicated increased infiltration of non-muscle cells upon injury. Together
709 these results support the hypothesis that TGF-β and myostatin act on fibroblasts and possibly
710 other cell types within the muscle tissue to induce expression of collagens. We previously
711 showed that inhibition of *Tgfbr1* in C2C12 myoblasts reduced *Ctgf* and *Col1a1* expression
712 (Hillege et al., 2020). Moreover, systemic administration of anti-TGF-β or soluble ACVR2B in
713 murine X-linked muscular dystrophy (mdx) mice reduced muscular fibrosis (Andreetta et al.,
714 2006; Bo Li, Zhang, & Wagner, 2012). In conclusion, to reduce expression of ECM components

715 within skeletal muscle inhibition of TGF-β signalling in other cell types such as fibroblasts and
716 satellite cells is required.

717 Chronic excessive ECM deposition leads to increased muscle stiffness and loss of
718 function. However, transiently enhanced ECM deposition is essential to early muscle
719 regeneration and results in scar free muscle repair in various types of acute injury (Hardy et al.,
720 2016; Mahdy, Lei, Wakamatsu, Hosaka, & Nishimura, 2015). In this study after CTX injury
721 *Col1a1* and *Col3a1* expression increased in all groups. Transient enhanced ECM deposition is
722 required to maintain muscle structural integrity and provides a scaffold for regenerating
723 myofibres (Kaariainen, Jarvinen, Jarvinen, Rantanen, & Kalimo, 2000). Furthermore,
724 interaction between fibroblasts and SCs appears to be essential for proper muscle regeneration,
725 since fibroblasts prevent early differentiation of SCs, while in turn SCs control the number of
726 fibroblasts (Murphy, Lawson, Mathew, Hutcheson, & Kardon, 2011). Thus the observed
727 enhanced expression of ECM components in TA that lacks both receptors may contribute to the
728 increased number of SCs at day 0 and acceleration of early muscle regeneration.

729

730 <u>Implications for ACVR1B and TGFBR1 inhibition as potential therapeutic strategy</u>

731 An important limitation of our study is that we are investigating effects of *Acvr1b* and *Tgfbr1*
732 knockout on early regeneration after an acute injury. In contrast to our model, a dystrophic or
733 aged mouse model has characteristics such as chronic inflammation, impaired regeneration and
734 fibrosis. Further research is required to determine how *Acvr1b* and *Tgfbr1* knockout affects long
735 term regeneration capacity, chronic inflammation and fibrosis in a pathological model.

736 Our data indicate that simultaneous knockout of *Acvr1b* and *Tgfbr1* in the mature
737 myofibre causes muscle hypertrophy and accelerates early muscle regeneration. The
738 inflammatory response is likely independent on TGF-β signalling within the myofibre.
739 Furthermore, specifically targeting *Tgfbr1* and *Acvr1b* in mature myofibre actually increased

740 relative ECM gene expression levels. This effect is likely the result of enhanced TGF-β
741 signalling in other cell types (i.e. fibroblasts and inflammatory cells). Thus, targeting TGF-β
742 signalling in immune cells and fibroblasts present in muscle tissue is likely required to alleviate
743 chronic inflammation and fibrosis.

744 Taken together, our data indicate that individually inhibiting either *Acvr1b* or *Tgfbr1*
745 may not be sufficient to alleviate muscle pathologies, nevertheless combined inhibition of both
746 *Acvr1b* and *Tgfbr1* may increase muscle mass and accelerate early muscle regeneration.

747 **Materials and Methods**

Key Resources Table				
Reagent type (species) or resource	Designation	Source or reference	Identifiers	Additional information
strain, strain background (include species and sex here)	C57BL/6	PMID: 22564549	# 025750	Jackson Laboratory, Bar Harbor, ME, USA
genetic reagent (include species here)	HSA-MCM	PMID: 22564549	# 025750	Jackson Laboratory, Bar Harbor, ME, USA
genetic reagent (include species here)	Acvr1b$^{fl/f}$	PMID: 23109354		Cancer Research Center of Lyon, French Institute of Health and Medical Research
genetic reagent (include species here)	Tgfbr1$^{fl/fl}$	PMID: 11285230		Leiden University Medical Center
antibody	Mouse anti-MHC-I	DSHB, Iowa City, IA, USA	BAD-5-s	IF (1 µg/mL)
antibody	Mouse anti-MHC-IIA	DSHB, Iowa City, IA, USA	SC-71	IF (10 µg/mL)

antibody	Mouse anti-MHC-IIB	DSHB, Iowa City, IA, USA	BF-F3	IF (1 µg/mL)
antibody	Mouse anti-MHC-IIX	DSHB, Iowa City, IA, USA	6H1	IF (1 µg/mL)
antibody	Mouse anti-Embryonic myosin heavy chain (eMyHc)	DSHB, Iowa City, IA, USA	F1.652-s	IF (20 µg/mL)
antibody	Mouse anti-Pax7	DSHB, Iowa City, IA, USA	PAX7	IF (4 µg/mL)
antibody	Rabbit anti-F4/80 (D4C8V) XP	Cell signaling, USA	#30325	IF (0.5 µg/mL)
antibody	Mouse anti-Myogenin	DSHB, Iowa City, IA, USA	F5D	IF (0.6 µg/mL)
antibody	Ki67	Rabbit mAb (Alexa Fluor 488 conjugate)	#1182	1:200
antibody	Goat anti-Mouse Alexa Fluor® 647 IgG_{2b}	Thermo Scientific, Waltham, MA, USA	A21242	IF (5 µg/mL)
antibody	Goat anti-Mouse Alexa Fluor® 488 IgG_1	Thermo Scientific, Waltham, MA, USA	A21121	IF (5 µg/mL)
antibody	Goat anti-Mouse Alexa Fluor® 647 IgM	Thermo Scientific, Waltham, MA, USA	A21238	IF (5 µg/mL)

antibody	Goat anti-Mouse Alexa Fluor® 488 IgM	Thermo Scientific, Waltham, MA, USA	A21042	IF (5 µg/mL)
antibody	Goat anti-Mouse Alexa Fluor® 488 IgG (H+L)	Thermo Scientific, Waltham, MA, USA	A11029	IF (4-5 µg/mL)
antibody	Anti-rabbit IgG (H+L), F(ab')2 Fragment Alexa Fluor® 488 Conjugate	Cell signaling, USA	#4412	IF (5 µg/mL)
sequence-based reagent	Rps13-F	This paper	PCR primers	CACGTGGCTGAAGTTG ACG
sequence-based reagent	Rps13-R	This paper	PCR primers	CAGGATTACACCTATC TGGGAGG
sequence-based reagent	Rpl27-F	This paper	PCR primers	AGCCGTCATCGTGAAG AAC
sequence-based reagent	Rpl27-R	This paper	PCR primers	GGGGATAGCGGTCAA TTCC
sequence-based reagent	Tgfbr1-F	This paper	PCR primers	CCTCGAGACAGGCCAT TTGT
sequence-based reagent	Tgfbr1-F	This paper	PCR primers	AGACGAAGCAGACTG GACCA
sequence-based reagent	Acvr1b-F	This paper	PCR primers	TGCTGCGCCATGAAAA CATC

sequence -based reagent	Acvr1b-F	This paper	PCR primers	TGCCCACAATCTCCAT ATGCA
sequence -based reagent	Tgf-β1-F	This paper	PCR primers	GCTGACCCCCACTGAT ACG
sequence -based reagent	Tgf-β1-R	This paper	PCR primers	CCTGTATTCCGTCTCC TTGGTT
sequence -based reagent	Mstn-F	This paper	PCR primers	GAGAATGGCCATGATC TTGCTG
sequence -based reagent	Mstn-R	This paper	PCR primers	CTTCTAAAAAGGGATT CAGCCCATC
sequence -based reagent	Igf1ea-F	This paper	PCR primers	GTGTTGCTTCCGGAGCT GTG
sequence -based reagent	Igf1ea-R	This paper	PCR primers	CAATGTACTTCCTTCT GAGTC
sequence -based reagent	Hgf-F	This paper	PCR primers	GATTATTGCCCTATTT CCCGTTGTG
sequence -based reagent	Hgf-R	This paper	PCR primers	TGGCACAGGATATTAC AGGATGG
sequence -based reagent	Mgf-F	This paper	PCR primers	GGAGAAGGAAAGGAA GTACATTTG

sequence -based reagent	Mgf-R	This paper	PCR primers	CCTGCTCCGTGGGAGG CT
sequence -based reagent	Vegf-F	This paper	PCR primers	CTGTAACGATGAAGCC CTGGAGTG
sequence -based reagent	Vegf-R	This paper	PCR primers	GGTGAGGTTTGATCCG CATGATCT
sequence -based reagent	Pax7-F	This paper	PCR primers	TCCATCAAGCCAGGA GACA
sequence -based reagent	Pax7-R	This paper	PCR primers	AGGAAGAAGTCCCAC ACAG
sequence -based reagent	Myod-F	This paper	PCR primers	CATCCAGCCCGCTCCA AC
sequence -based reagent	Myod-R	This paper	PCR primers	GGGCCGCTGTAATCCA TCATGCC
sequence -based reagent	Myog-F	This paper	PCR primers	CCCAACCCAGGAGAT CATTT
sequence -based reagent	Myog-R	This paper	PCR primers	GTCTGGGAAGGCAAC AGACA
sequence -based reagent	Myh3-F	This paper	PCR primers	CGCAGAATCGCAAGT CAATA

sequence -based reagent	Myh3-R	This paper	PCR primers	CAGGAGGTCTTGCTCA CTCC
sequence -based reagent	Id1-F	This paper	PCR primers	ACCCTGAACGGCGAG ATCA
sequence -based reagent	Id1-R	This paper	PCR primers	TCGTCGGCTGGAACAC AT
sequence -based reagent	Fgf2-F	This paper	PCR primers	AAGCGGCTCTACTGCA AGAA
sequence -based reagent	Fgf2-R	This paper	PCR primers	GTAACACACTTAGAA GCCAGCAG
sequence -based reagent	Ctgf-F	This paper	PCR primers	CCACCCGAGTTACCAA TGAC
sequence -based reagent	Ctgf-R	This paper	PCR primers	GCTTGGCGATTTTAGG TGTC
sequence -based reagent	Col1a1-F	This paper	PCR primers	ATGTTCAGCTTTGTGGA CCT
sequence -based reagent	Col1a1-R	This paper	PCR primers	CAGCTGACTTCAGGGA TGT
sequence -based reagent	Col3a1-F	This paper	PCR primers	AAGGACATCGAGGAT TCCCTG

sequence -based reagent	Col3a1-R	This paper	PCR primers	AGCCCTCAGATCCTCT TTCAC
sequence -based reagent	Cd68-F	This paper	PCR primers	TCCCAACAAAACCAA GGTCCA
sequence -based reagent	Cd68-R	This paper	PCR primers	GGCTCTGATGTAGGTC CTGTTT
sequence -based reagent	Cd163-F	This paper	PCR primers	CGGCCCCATGAAGAG GTATC
sequence -based reagent	Cd163-R	This paper	PCR primers	GACGGTTGACCCAGTT GTTG
sequence -based reagent	Il-1β-F	This paper	PCR primers	GCCACCTTTTGACAGT GATG
sequence -based reagent	Il-1β-R	This paper	PCR primers	CTTCTCCACAGCCACA ATGA
sequence -based reagent	Il-6-F	This paper	PCR primers	GGAAATGAGAAAAGA GTTGTGC
sequence -based reagent	Il-6-R	This paper	PCR primers	GTACTCCAGAAGACC AGAGGA
sequence -based reagent	Atrogin-1-F	This paper	PCR primers	AGACTGGACTTCTCGA CTGC

sequence -based reagent	Atrogin-1-R	This paper	PCR primers	TCAGCTCCAACAACAG CCTTACT
sequence -based reagent	Murf-1-F	This paper	PCR primers	CGTCCAGAGCGTGTGT CTCACTC
sequence -based reagent	Murf-1-R	This paper	PCR primers	GGGCTACCTTCCTCTC AAGTGC
sequence -based reagent	Tcf4-F	This paper	PCR primers	GGAAAGCCCTAGCTTC GATCT
sequence -based reagent	Tcf4-R	This paper	PCR primers	GGAGCCCACAGGAGT TGAA
sequence -based reagent	Pdgfra-F	This paper	PCR primers	ACTTTTCACTCCGGGT ATCGG
sequence -based reagent	Pdgfra-R	This paper	PCR primers	CCCATAGCTCCTGAGA CCTTC
commerc ial assay or kit	RiboPure™ RNA Purification Kit	Thermo Fisher Scientific	AM1924	
commerc ial assay or kit	SuperScript VILO Mastermix	Thermo Fisher Scientific	12023679	

748

749

750 Animal housing and welfare

751 The HSA-MCM transgenic mouse line (McCarthy et al., 2012b) was obtained from Jackson

752 Laboratory, Bar Harbor, ME,USA (stock number # 025750), the Acvr1b$^{fl/fl}$ mouse line

753 (Ripoche et al., 2013) was obtained from Philippe Bertolino (Cancer Research Center of Lyon,
754 French Institute of Health and Medical Research) and the Tgfbr1$^{fl/fl}$ mouse line (Larsson et al.,
755 2001) was provided by Peter ten Dijke (Leiden University Medical Center). All mouse lines
756 were of a C57BL/6 background. Mouse lines were cross-bred in house to obtain mouse lines
757 HSA-MCM:Acvr1b$^{fl/fl}$, HSA-MCM:Tgfbr1$^{fl/fl}$ and HSA-MCM:Acvr1b$^{fl/fl}$:Tgfbr1$^{fl/fl}$. Animals
758 were housed in a controlled 12 hours light-dark cycle (light on 6:00-18:00 GMT + 1h) with a
759 temperature of 21 ± 1°C and a humidity between 40 and 70%. Food (Teklad, Envigo, Horst,
760 The Netherlands) and water were available at libitum. All experiments were performed
761 according to the national guidelines approved by the Central Committee for Animal
762 Experiments (CCD) (AVD112002017862) and the Institute of Animal Welfare (IvD) of the
763 Vrije Universiteit Amsterdam.
764
765 Genotyping
766 In these mouse models, skeletal myofibre specific Cre expression is driven by the HSA
767 promoter which can be activated by TMX, resulting in the deletion of targeted exon of 5 and 6
768 of *Acvr1b* and exon 3 of *Tgfbr1* resulting in a targeted knockout of the gene. Genotyping for
769 the HSA-MCM, Acvr1b$^{fl/fl}$ and Tgfbr1$^{fl/fl}$ genes was performed by isolating DNA from ear
770 biopsies of offspring and PCR was performed in a 2720 thermal cycler (Applied Biosystems,
771 Foster City, CA, USA). PCR master mix per sample was prepared by mixing 0.2 µl of
772 AmpliTaq Gold DNA polymerase, 2.5 µl of gold buffer, 1.5 µl of $MgCl_2$ (Thermo Fisher
773 Scientific, 4311806, Waltham, MA, USA), 0.5 µl of dNTPs (100mM diluted 10×, Invitrogen
774 10297018, Carlsbad, CA, USA), 1 µl of each primer diluted in DNAse/RNAse free water to
775 obtain a volume of 23 µl Master mix per sample. 2 µl DNA was added per sample. The
776 following PCR programs were used: for HSA-MCM and Acvr1b$^{fl/fl}$: 94°C for 5 minutes,
777 followed by a 35× cycle of 94°C for 30 seconds, 58°C for 30 seconds and 72°C for 10 minutes,

778 finishing with 72°C for 10 minutes and cooled down to 4°C. PCR program for Tgfbr1$^{fl/fl}$: 94°C
779 for 4 minutes, followed by a 35× cycle of 94°C for 30 seconds, 50°C for 45 seconds and 72°C
780 for 1 minute, finishing with 72°C for 5 minutes and cooled down to 4°C. Amplified DNA was
781 mixed with 5 µl loading buffer and samples were loaded in a 4% agarose gel using SYBR safe
782 DNA gel staining 1000× concentrate (Thermo Fisher Scientific s33102, Waltham, MA, USA),
783 DNA was separated by electrophoresis (25 minutes, 75 V) and gel image was taken using an
784 Image Quant LAS 500 chemo luminescence CCD camera (GE healthcare, life sciences,
785 Chicago, IL, USA).
786 Primer sequences: HSA-MCM gene: Forward, 5′- GCATGGTGGAGATCTTTGA-3′
787 (McCarthy et al., 2012b) and Reverse, 5′-CGACCGGCAAACGGACAGAAGC-'3 (McCarthy,
788 Srikuea, Kirby, Peterson, & Esser, 2012a). Acvr1b$^{fl/fl}$ gene: Acvr1b In4, 5'-
789 CAGTGGTTAAGAACACTGGC-3', Acvr1b In5, 5'- GTAGTGTTATGTGTTATTGCC -3'
790 And Acvr1b In6, 5'GAGCAAGAGTTTCTCTATGTAG-3' (Ripoche et al., 2013). Tgfbr1$^{fl/fl}$
791 gene: Forward, 5'- CCTGCAGTAAACTTGGAATAAGAAG-'3, reverse, 5'-
792 GACCATCAGCTGTCAGTACCC-3' (Protocol 19216: Standard PCR Assay -
793 Tgfbr1<tm1.1Karl>, Jackson Laboratory, Bar Harbor, ME,USA).
794

795 Cardiotoxin induced injury assay

796 Animals of each genotype were assigned to each timepoint randomly to ensure that groups were
797 on average the same age at the time of the first TMX injection. Littermates were assigned to
798 different timepoints. Six weeks old HSA-MCM:Acvr1b$^{fl/fl}$, HSA-MCM:Tgfbr1$^{fl/fl}$, HSA-
799 MCM:Acvr1b$^{fl/fl}$:Tgfbr1$^{fl/fl}$ and HSA-MCM Cre^{+} male mice were injected intraperitoneally
800 with 100 mg/kg/day tamoxifen (Sigma-Aldrich, T5648, Saint-Louis, MO, USA) in sunflower
801 oil (10 mg/ml) for five consecutive days. Five weeks post TMX injections, mice were injected
802 intramuscularly in the TA muscles of both hind limbs with 20 µl CTX from Naja pallida

803 (Latoxan Laboratory, L8102, Portes les Valence, France) in phosphate buffered saline (PBS)
804 (10 µM). CTX was slowly injected (1 µl/s) into mid muscle belly using a Hamilton syringe
805 with attached 34G needle inserted in a 15-25° angle, 2-3 mm deep. Mice were shortly
806 anesthetised using isoflurane 1.5-3% on a warm blanket during the injections. Mice were
807 divided into three groups: mice that were sacrificed 2 days or 4 days post injury and mice with
808 no CTX injection, that were sacrificed at day 0, which functioned as a baseline control. Mice
809 were sacrificed by cervical dislocation and TA muscles were isolated and frozen in isopentane
810 cooled in liquid nitrogen. Each subgroup contained 5-8 mice.
811
812 RNA isolation and reverse transcription
813 Whole TA muscle was used for RNA isolation. 50 mg cryopreserved TA muscle was
814 homogenised (Potter S 8533024, B. BRAUN) in 700 µl TRI reagent (Invitrogen, 11312940,
815 Carlsbad, CA, USA) and incubated at room temperature (RT) for 5 minutes. Samples were
816 centrifuged for 10 minutes (4°C, 12000 g). Supernatant was transferred to a new tube and 70
817 µl bromochloropropane (Sigma-Aldrich, B9673, Saint Louis, MO, USA) was added. Lysates
818 were inverted and incubated at RT for 5 minutes and centrifuged (4°C, 12000 g, 10 minutes).
819 RNA containing supernatant was transferred to a new centrifuge tube and washed with 100%
820 ethanol 2:1. RNA was further isolated using the RiboPure RNA purification kit (Thermo Fisher
821 Scientific, AM1924, Waltham, MA, USA). Then, 500 ng RNA and 4 µl SuperScript VILO
822 Mastermix (Invitrogen, 12023679, Carlsbad, CA, USA) were diluted to 20 µl in RNAse free
823 water and reverse transcription was performed in a 2720 thermal cycler (Applied Biosystems,
824 Foster City, CA, USA), using the following program: 10 minutes at 25 °C, 60 minutes at 42 °C
825 and 5 minutes at 85 °C. cDNA was diluted 10× in RNAse free water.
826
827 Quantitative real time PCR

828 5 µl of PowerUp SYBR Green master mix (Applied Biosystems, A25742, Foster City, CA,
829 USA), 3 µl of primer mix and 2 µl of cDNA were added in duplo in a 96 wells plate. The
830 program ran on the Quant Studio 3 real time PCR (Applied Biosystems, Foster City, CA, USA)
831 was 2 minutes at 50°C, 2 minutes at 95°C, 40× 1 second at 95°C and 30 seconds at 60°C, 15
832 seconds at 95°C, 1 minute at 60°C and 15 seconds at 95°C. Geometric mean of reference genes
833 ribosomal protein S13 (*Rps13*) and ribosomal protein L27 (*Rpl27*) was used to correct for
834 cDNA input. The efficiency of all primers sequences (Key Resources Table) was > 98%.
835
836 Western blot
837 Fifty 20 µm cross sections of TA and EDL muscles were obtained using a cryostat microtome
838 (Microm HM550, Adamas Instruments, Rhenen, The Netherlands). GM tissue and whole EDL
839 muscles were lysed (Potter S 8533024, B. BRAUN) in RIPA buffer (Sigma-Aldrich, R0278,
840 Saint Louis, MO, USA) containing 1 tablet of protease inhibitor (Sigma-Aldrich, 11836153001)
841 and 1 tablet of phosStop (Sigma-Aldrich, 04906837001) per 10ml. The total protein
842 concentration in the lysates was determined using a Pierce BCA Protein Assay kit (Thermo
843 Scientific, 23225). A 4–20% Mini-PROTEAN® TGX™ Precast Protein Gels was used. 15µl
844 sample mix containing 12µg total protein and 4µl sample buffer (4× Laemmli Sample Buffer,
845 Bio-Rad, 1610747) with 10% mercaptoethanol (Bio-Rad, 1610710) was heated to 95ºC for 5
846 minutes, cooled on ice and loaded onto the gel. After electrophoresis, proteins were transferred
847 onto a polyvinylidene fluoride (PVDF) membrane (GE Healthcare, 15269894) for blotting at
848 80V for 60 minutes. The membrane was incubated for 1 hour at RT in 2% enhanced
849 chemiluminiscence (ECL) prime blocking agent (GE Healthcare, RPN418). Membranes were
850 incubated overnight at 4ºC in blocking buffer (4% bovine serum albumin (BSA) in tris-buffered
851 saline with 0.1% Tween 20 detergent (TBST)) with primary antibody at a dilution of 1:500 for
852 Phospho-Smad2 (Ser465/467) (138D4) (Rabbit mAb, 3108, Cell signaling, USA), 1:500

853 Phospho-Smad3 (Ser423/425) (C25A9) (Rabbit mAb, 9520, Cell signalling, USA), 1:500 for
854 Purified mouse anti-Smad2/3 (610843, BD Biosciences, USA), 1:1000 for Phospho-AKT
855 (Ser473) (Rabbit mAb, 4060, Cell signaling, USA) , 1:2000 for AKT (pan) (C67E7) (Rabbit
856 mAb, 4691, Cell signaling, USA), Phospho-p70S6 Kinase (Thr389) (108D2) (Rabbit mAb,
857 8209, Cell signaling, USA), p70S6 Kinase (49D7) (Rabbit mAb, 2708, Cell signaling, USA)
858 and Pan-Actin (Rabbit Ab, 4968, Cell signalig, USA). Incubation with secondary antibody,
859 anti-Rabbit IgG-POD, (P0448, Agilent Dako, USA) or Rabbit anti-Mouse IgG, IgM (H+L),
860 HRP conjugate (31457, ThermoFisher Scientific, USA) at a dilution of 1:2000 was done for 1
861 hour at RT in blocking buffer and detection was done using ECL detection kit (RPN2235, GE
862 Healthcare, USA). Images were taken by the ImageQuant LAS500 (GE healthcare, life
863 sciences, USA) and relative intensity of protein bands was quantified using ImageJ (Schneider,
864 Rasband, & Eliceiri, 2012). Pan-Actin was used as a loading control.
865
866 Tissue cross sectioning for histological analysis
867 For histological analysis, 10 µm thick cross-sections of TA or EDL muscles were obtained
868 using a cryostat microtome (Microm HM550, Adamas Instruments, Rhenen, The Netherlands),
869 mounted on microscope slides (super frost plus, Thermo Scientific, J1800AMNZ, Landsmeer,
870 The Netherlands) and stored at -80°C for further analyses. In addition, for TA muscle, 10 µm
871 thick longitudinal sections were obtained to measure the myonuclear length.
872
873 Histochemistry staining of H&E and Sirius Red staining
874 For H&E staining, slides with muscle sections were air dried for 10 minutes. Dried slides were
875 then stained in Hematoxylin for 2 minutes, then washed under tap water for 15 minutes and
876 further stained in Eosin for 1 minute. Immediately after Eosin staining, slides were rinsed 2× in
877 100% alcohol for 10 seconds and 2× in xylene for 10 minutes. Stained sections were mounted

878 in Entellan (Merck, 107960, Darmstadt, Germany), covered with coverslip and dried overnight
879 before analysis.
880 For Sirius Red staining, sections were air dried for 10 minutes at RT, then they were
881 fixed in acetone at -20°C for 10 minutes and subsequently fixed in saturated Bouin for 30
882 minutes at RT. Samples were stained by Sirius Red for 30 minutes and washed in 0.01 M
883 hydrochloric acid. Then, sections were rapidly dehydrated in 100% ethanol and xylene twice.
884 Stained sections were mounted in Entellan, covered with coverslip and dried overnight before
885 analysis (de Bruin, Smeulders, Kreulen, Huijing, & Jaspers, 2014).
886 Images were captured on a Zeiss Axioskop microscope (Carl Zeiss BV, Breda The
887 Netherlands) with Basler camera (Basler AG, Ahrensburg, Germany) using Manual WSI
888 scanner software (Microvisioneer) for collecting whole scan images. Regeneration area
889 percentage at day 0 was referred to area of myofibres with central nuclei divided by total area
890 of a whole muscle cross-section. Morphometry was performed using ImageJ software
891 (Schneider et al., 2012).
892
893 Immunofluorescence staining
894 Microscope slides with muscle sections were air dried for 10 minutes. For Pax7 staining,
895 sections were fixed with 4% paraformaldehyde (PFA) at RT for 10 minutes and washed in PBS-
896 T (0.05% Tween 20). Sections were blocked at RT with 10% normal goat serum (NGS)
897 (Thermo Fisher Scientific, 50062Z, Waltham, MA, USA) (60 minutes for myosin heavy chain
898 (MyHC), eMyHC, F4/80 and Myogenin staining, or 30 minutes for Pax7 staining) or 5% NGS
899 with 0.3% Triton-X100 for 60 minutes for Ki67/Pax7 staining. Sections for Pax7 staining were
900 subsequently blocked in 1% BSA in PBS for 30 minutes. Sections were incubated in primary
901 antibodies (Key Resources Table) in 10% NGS (for MyHC, eMyHC or Myogenin) or in 0.1%
902 BSA (Pax7, F4/80 or Ki67/Pax7) at RT for 60 minutes or overnight. Then sections were

903 incubated in secondary antibodies (Key Resources Table) in 10% NGS for MyHC and eMyHC
904 staining, or in 0.1% BSA for Pax7 or F4/80 staining at RT in the dark for 60 minutes. After
905 this, sections were incubated in 1:50 diluted wheat germ agglutinin (WGA) (Fisher Scientific,
906 11590816, Pittsburgh, PA, USA) in PBS at RT for 20 minutes. Finally, slides were carefully
907 dried and mounted with Vectashield hardset mounting medium with 4‘,6-diamidino-2-
908 phenylindole (DAPI) (Brunschwig, H1500, Amsterdam, The Netherlands). Slides were dried
909 overnight at 4°C.
910
911 Immunofluorescence microscopy and analysis
912 Images of all immunofluorescence assays were captured using a fluorescent microscope (Zeiss
913 Axiovert 200M, Hyland Scientific, Stanwood, WA, USA) with a PCO SensiCam camera (PCO,
914 Kelheim, Germany) using the program Slidebook 5.0 (Intelligent Imaging Innovations,
915 Göttingen, Germany). The images were analysed using ImageJ (Schneider et al., 2012).
916 Individual images were taken across the entire cross-section and assembled into a composite
917 panoramic image. For TA, the inner part of the muscle tissue was referred to as high oxidative
918 region and the outer part was referred to as low oxidative region. For myofibre type analysis,
919 250 myofibres within each part were characterised in TA. Hybrid myofibre fluorescence was
920 assessed by myofibres stained by double colours and pure myofibres were determined by single
921 colour staining (Bloemberg & Quadrilatero, 2012). To determine CSA per myofibre type, CSA
922 was measured of 30 myofibres per type, or as many as were present within the tissue per TA.
923 For EDL, myofibre type and CSA of all myofibres within the muscle were determined by
924 SMASH (L. R. Smith & Barton, 2014). Within images stained for Pax7, the number of $Pax7^+$
925 nuclei and the number of myofibres were determined in the low oxidative region of TA from
926 about 200 myofibres (5 fields per specimen). SCs were defined as $Pax7^+$ cells that were located
927 between plasma and basal lamina of myofibre (Lindstrom & Thornell, 2009). Within muscle

928 sections images stained for F4/80, the density of macrophages in TA at day 0 was determined
929 in 10 randomly selected locations in TA at day 0 and at least 3 locations within the injured
930 region at day 2 and 4 after injury. Macrophages were defined as F4/80$^+$ cells that were located
931 in the interstitial region of the myofibres at day 0. To measure the number of myonuclei per
932 type IIB myofibre, 100 type IIB myofibres in the low oxidative region were taken into account
933 and nuclei were considered as myonuclei when they were located within the cytoplasm below
934 the basal lamina. To determine myonuclear length, images were taken at 10 × magnification
935 using a fluorescent microscope. Mean myonuclear length was determined as the average value
936 of 30 nuclei. For regeneration analysis, myofibre CSA measurement was performed by
937 outlining 50 eMyHC$^+$ myofibres from three randomly chosen fields within the regenerating
938 area in muscle cross-sections of day 4. RI was defined as the number of nuclei within eMyHC$^+$
939 myofibres divided by the number of eMyHC$^+$ myofibres, all eMyHC$^+$ myofibres in three
940 randomly chosen fields (1.38mm^2 per field) within the regenerating area were included in the
941 analysis. The densities of Ki67$^+$, Pax7$^+$, Ki67$^+$/Pax7$^+$ and Myogenin$^+$ cells in TA were
942 determined by counting the number of cells per mm^2 of muscle CSA. Ten images in low
943 oxidative region of TA on day 0, 2 and 4 were randomly selected. All analyses were performed
944 at 20× magnification.
945
946 <u>SDH assay</u>
947 Succinate dehydrogenase activity was quantified according to Van der Laarse (1989). Breiefly,
948 freshly muscle cross-sections (10 µm thick) were air dried for 15 minutes at RT. Sections were
949 incubated in prewarmed SDH (37.5 mM $NaH_2PO_4 \cdot H_2O$, 37.5 mM $Na_2HPO_4 \cdot 2H_2O$, added acid
950 to pH 7.6, 75 mM sodium succinate, 5 mM NaN_3, 0.5 g/L tetranitroblue tetrazolium (TNBT))
951 medium for 10 minutes at 37°C. Sections were rinsed 3 seconds in 0.01 M hydrochloric acid.
952 Then sections were rinsed for 1 minute twice in ultrapure water. Finally, sections were mounted

953 in glycerine gelatin (Merck, 48723, Darmstadt, Germany) with coverslips and dried overnight
954 before analysis. Images were captured by a Leica DMRB microscope (Wetzlar, Germany) with
955 calibrated grey filters and a CCD camera (Sony XC77CE, Towada, Japan) connected to a LG-
956 3 frame grabber (Scion, Frederick, MD, United States). The absorbances of the SDH-reaction
957 product in the sections were determined at 660 nm using a calibrated microdensitometer and
958 ImageJ (Schneider et al., 2012). SDH activity ($\Delta A_{660} \cdot \mu m^{-1} \cdot s^{-1}$) was measured by the rate of
959 absorbance per section thickness per second ($\Delta A_{660}/(10\ \mu m \cdot 600s)$) after subtracting
960 background activity in 5 locations in low oxidative region at 10× magnification. The integrated
961 SDH activity ($\Delta A_{660} \cdot \mu m \cdot s^{-1}$) was defined as SDH activity × myofibre CSA. Absorbance was
962 measured in a total of 50 myofibres per TA.
963
964 Statistical analysis
965 Graphs were made in Prism version 8 (GraphPad software, San Diego, CA, USA). All data
966 were presented as mean + standard error of the mean (SEM). Statistical analysis was performed
967 in SPSS version 26 (IBM, Amsterdam, The Netherlands). Sample size was determined a priori,
968 based on previously published *in vivo* research on TGF-β and myostatin. Statistical significance
969 for multiple comparisons was determined by two-way analysis of variance (ANOVA), three-
970 way ANOVA or independent t-test. Significance was set at $P < 0.05$. Data normality was tested
971 with a Shapiro-Wilk test ($P < 0.05$). Homogeneity of variance was tested with a Levene's test
972 ($P < 0.01$). If necessary, data were square or log transformed. Post hoc Bonferroni or Games-
973 Howell corrections were performed. If normality was violated a Kruskall Wallis test was
974 performed.
975
976 Data availability
977 This study includes data deposited in Dryad.

Acknowledgements

This research was funded by the Prinses Beatrix Spierfonds, grant number W.OR14-17 and a grant from the China Scholarship Council (CSC grant number 201808440351). We thank Philippe Bertolino (Cancer Research Center of Lyon, French Institute of Health and Medical Research) and Peter ten Dijke (Leiden University Medical Center) for providing the Acvr1b$^{fl/fl}$ and Tgfbr1$^{fl/fl}$ mouse lines. We thank animal caretakers of the Universitair Proefdier Centrum of the Vrije Universiteit Amsterdam, our colleague Wendy Noort and students Elke Schmitz and Bijee Visbeek for their contribution to data analysis.

Author contributions

Conceptualization and Methodology: M.M.G.H., A.S., R.A.G., W.M.H.H., R.T.J.

Formal Analysis: M.M.G.H., A.S.

Funding acquisition: R.T.J, W.M.H.H.

Investigation: M.M.G., A.S., R.A.G.

Resources: R.T.J., P.B.

Supervision: G.W., R.T.J.

Visualization and Writing – original draft: M.M.G.H., A.S.

Writing – review & editing: M.M.G.H., A.S., R.A.G., W.M.H.H., R.T.J.

Conflict of interests

Authors declare no conflict of interests.

References

Accornero, F., Kanisicak, O., Tjondrokoesoemo, A., Attia, A. C., McNally, E. M., & Molkentin, J. D. (2014). Myofiber-specific inhibition of TGFbeta signaling protects skeletal muscle from injury and dystrophic disease in mice. *Hum Mol Genet, 23*(25), 6903-6915. doi:10.1093/hmg/ddu413

Allen, R. E., & Boxhorn, L. K. (1989). Regulation of skeletal muscle satellite cell proliferation and differentiation by transforming growth factor-beta, insulin-like growth factor I, and fibroblast growth factor. *J Cell Physiol, 138*(2), 311-315. doi:10.1002/jcp.1041380213

Allen, R. E., Sheehan, S. M., Taylor, R. G., Kendall, T. L., & Rice, G. M. (1995). Hepatocyte growth factor activates quiescent skeletal muscle satellite cells in vitro. *J Cell Physiol, 165*(2), 307-312. doi:10.1002/jcp.1041650211

Amirouche, A., Durieux, A. C., Banzet, S., Koulmann, N., Bonnefoy, R., Mouret, C., . . . Freyssenet, D. (2009). Down-regulation of Akt/mammalian target of rapamycin signaling pathway in response to myostatin overexpression in skeletal muscle. *Endocrinology, 150*(1), 286-294. doi:10.1210/en.2008-0959

Amthor, H., Macharia, R., Navarrete, R., Schuelke, M., Brown, S. C., Otto, A., . . . Patel, K. (2007). Lack of myostatin results in excessive muscle growth but impaired force generation. *Proc Natl Acad Sci U S A, 104*(6), 1835-1840. doi:10.1073/pnas.0604893104

Andreetta, F., Bernasconi, P., Baggi, F., Ferro, P., Oliva, L., Arnoldi, E., . . . Confalonieri, P. (2006). Immunomodulation of TGF-beta 1 in mdx mouse inhibits connective tissue proliferation in diaphragm but increases inflammatory response: implications for antifibrotic therapy. *J Neuroimmunol, 175*(1-2), 77-86. doi:10.1016/j.jneuroim.2006.03.005

Arnold, L., Henry, A., Poron, F., Baba-Amer, Y., van Rooijen, N., Plonquet, A., . . . Chazaud, B. (2007). Inflammatory monocytes recruited after skeletal muscle injury switch into antiinflammatory macrophages to support myogenesis. *J Exp Med, 204*(5), 1057-1069. doi:10.1084/jem.20070075

Arsic, N., Zacchigna, S., Zentilin, L., Ramirez-Correa, G., Pattarini, L., Salvi, A., . . . Giacca, M. (2004). Vascular endothelial growth factor stimulates skeletal muscle regeneration in vivo. *Mol Ther, 10*(5), 844-854. doi:10.1016/j.ymthe.2004.08.007

Assoian, R. K., Fleurdelys, B. E., Stevenson, H. C., Miller, P. J., Madtes, D. K., Raines, E. W., . . . Sporn, M. B. (1987). Expression and secretion of type beta transforming growth factor by activated human macrophages. *Proc Natl Acad Sci U S A, 84*(17), 6020-6024. doi:10.1073/pnas.84.17.6020

Babcock, L. W., Knoblauch, M., & Clarke, M. S. (2015). The role of myostatin and activin receptor IIB in the regulation of unloading-induced myofiber type-specific skeletal muscle atrophy. *J Appl Physiol (1985), 119*(6), 633-642. doi:10.1152/japplphysiol.00762.2014

Bencze, M., Periou, B., Baba-Amer, Y., & Authier, F. J. (2019). Immunolabelling Myofiber Degeneration in Muscle Biopsies. *J Vis Exp*(154). doi:10.3791/59754

Bernasconi, P., Torchiana, E., Confalonieri, P., Brugnoni, R., Barresi, R., Mora, M., . . . Mantegazza, R. (1995). Expression of transforming growth factor-beta 1 in dystrophic patient muscles correlates with fibrosis. Pathogenetic role of a fibrogenic cytokine. *J Clin Invest, 96*(2), 1137-1144. doi:10.1172/JCI118101

Bloemberg, D., & Quadrilatero, J. (2012). Rapid determination of myosin heavy chain expression in rat, mouse, and human skeletal muscle using multicolor immunofluorescence analysis. *PLoS One, 7*(4), e35273. doi:10.1371/journal.pone.0035273

1050 Bo Li, Z., Zhang, J., & Wagner, K. R. (2012). Inhibition of myostatin reverses muscle fibrosis
1051 through apoptosis. *J Cell Sci, 125*(Pt 17), 3957-3965. doi:10.1242/jcs.090365
1052 Campbell, C., McMillan, H. J., Mah, J. K., Tarnopolsky, M., Selby, K., McClure, T., . . . Attie,
1053 K. M. (2017). Myostatin inhibitor ACE-031 treatment of ambulatory boys with
1054 Duchenne muscular dystrophy: Results of a randomized, placebo-controlled clinical
1055 trial. *Muscle Nerve, 55*(4), 458-464. doi:10.1002/mus.25268
1056 Cantini, M., Massimino, M. L., Rapizzi, E., Rossini, K., Catani, C., Dalla Libera, L., & Carraro,
1057 U. (1995). Human satellite cell proliferation in vitro is regulated by autocrine secretion
1058 of IL-6 stimulated by a soluble factor(s) released by activated monocytes. *Biochem*
1059 *Biophys Res Commun, 216*(1), 49-53. doi:10.1006/bbrc.1995.2590
1060 Carlson, M. E., Hsu, M., & Conboy, I. M. (2008). Imbalance between pSmad3 and Notch
1061 induces CDK inhibitors in old muscle stem cells. *Nature, 454*(7203), 528-532.
1062 doi:10.1038/nature07034
1063 Charge, S. B., & Rudnicki, M. A. (2004). Cellular and molecular regulation of muscle
1064 regeneration. *Physiol Rev, 84*(1), 209-238. doi:10.1152/physrev.00019.2003
1065 Chaweewannakorn, C., Tsuchiya, M., Koide, M., Hatakeyama, H., Tanaka, Y., Yoshida, S., . .
1066 . Kanzaki, M. (2018). Roles of IL-1alpha/beta in regeneration of cardiotoxin-injured
1067 muscle and satellite cell function. *Am J Physiol Regul Integr Comp Physiol, 315*(1),
1068 R90-R103. doi:10.1152/ajpregu.00310.2017
1069 Chen, A. L., Ou, C. W., He, Z. C., Liu, Q. C., Dong, Q., & Chen, M. S. (2012). Effect of
1070 hepatocyte growth factor and angiotensin II on rat cardiomyocyte hypertrophy. *Braz J*
1071 *Med Biol Res, 45*(12), 1150-1156. doi:10.1590/s0100-879x2012007500159
1072 Chen, J. L., Walton, K. L., Hagg, A., Colgan, T. D., Johnson, K., Qian, H., . . . Harrison, C. A.
1073 (2017). Specific targeting of TGF-beta family ligands demonstrates distinct roles in the
1074 regulation of muscle mass in health and disease. *Proc Natl Acad Sci U S A, 114*(26),
1075 E5266-E5275. doi:10.1073/pnas.1620013114
1076 Chen, J. L., Walton, K. L., Winbanks, C. E., Murphy, K. T., Thomson, R. E., Makanji, Y., . . .
1077 Gregorevic, P. (2014). Elevated expression of activins promotes muscle wasting and
1078 cachexia. *FASEB J, 28*(4), 1711-1723. doi:10.1096/fj.13-245894
1079 Choi, W., Lee, J., Lee, J., Ko, K. R., & Kim, S. (2018). Hepatocyte Growth Factor Regulates
1080 the miR-206-HDAC4 Cascade to Control Neurogenic Muscle Atrophy following
1081 Surgical Denervation in Mice. *Mol Ther Nucleic Acids, 12*, 568-577.
1082 doi:10.1016/j.omtn.2018.06.013
1083 Coleman, M. E., DeMayo, F., Yin, K. C., Lee, H. M., Geske, R., Montgomery, C., & Schwartz,
1084 R. J. (1995). Myogenic vector expression of insulin-like growth factor I stimulates
1085 muscle cell differentiation and myofiber hypertrophy in transgenic mice. *J Biol Chem,*
1086 *270*(20), 12109-12116. doi:10.1074/jbc.270.20.12109
1087 Conceicao, M. S., Vechin, F. C., Lixandrao, M., Damas, F., Libardi, C. A., Tricoli, V., . . .
1088 Ugrinowitsch, C. (2018). Muscle Fiber Hypertrophy and Myonuclei Addition: A
1089 Systematic Review and Meta-analysis. *Med Sci Sports Exerc, 50*(7), 1385-1393.
1090 doi:10.1249/MSS.0000000000001593
1091 Costelli, P., Muscaritoli, M., Bonetto, A., Penna, F., Reffo, P., Bossola, M., . . . Rossi Fanelli,
1092 F. (2008). Muscle myostatin signalling is enhanced in experimental cancer cachexia.
1093 *Eur J Clin Invest, 38*(7), 531-538. doi:10.1111/j.1365-2362.2008.01970.x
1094 da Silva, R. P., Platt, N., de Villiers, J. S., & Gordon, S. (1996). Membrane molecules and
1095 macrophage endocytosis: scavenger receptor and macrosialin as markers of plasma-
1096 membrane and vacuolar functions. *Biochem Soc Trans, 24*(1), 220-224.
1097 doi:10.1042/bst0240220

de Bruin, M., Smeulders, M. J., Kreulen, M., Huijing, P. A., & Jaspers, R. T. (2014). Intramuscular connective tissue differences in spastic and control muscle: a mechanical and histological study. *PLoS One, 9*(6), e101038. doi:10.1371/journal.pone.0101038

Delaney, K., Kasprzycka, P., Ciemerych, M. A., & Zimowska, M. (2017). The role of TGF-beta1 during skeletal muscle regeneration. *Cell Biol Int, 41*(7), 706-715. doi:10.1002/cbin.10725

Gal-Levi, R., Leshem, Y., Aoki, S., Nakamura, T., & Halevy, O. (1998). Hepatocyte growth factor plays a dual role in regulating skeletal muscle satellite cell proliferation and differentiation. *Biochim Biophys Acta, 1402*(1), 39-51. doi:10.1016/s0167-4889(97)00124-9

Gillies, A. R., & Lieber, R. L. (2011). Structure and function of the skeletal muscle extracellular matrix. *Muscle Nerve, 44*(3), 318-331. doi:10.1002/mus.22094

Girgenrath, S., Song, K., & Whittemore, L. A. (2005). Loss of myostatin expression alters fiber-type distribution and expression of myosin heavy chain isoforms in slow- and fast-type skeletal muscle. *Muscle Nerve, 31*(1), 34-40. doi:10.1002/mus.20175

Goodman, C. A., McNally, R. M., Hoffmann, F. M., & Hornberger, T. A. (2013). Smad3 induces atrogin-1, inhibits mTOR and protein synthesis, and promotes muscle atrophy in vivo. *Mol Endocrinol, 27*(11), 1946-1957. doi:10.1210/me.2013-1194

Grabiec, K., Tokarska, J., Milewska, M., Blaszczyk, M., Gajewska, M., & Grzelkowska-Kowalczyk, K. (2013). Interleukin-1beta stimulates early myogenesis of mouse C2C12 myoblasts: the impact on myogenic regulatory factors, extracellular matrix components, IGF binding proteins and protein kinases. *Pol J Vet Sci, 16*(2), 255-264. doi:10.2478/pjvs-2013-0036

Greco, S. H., Tomkotter, L., Vahle, A. K., Rokosh, R., Avanzi, A., Mahmood, S. K., . . . Miller, G. (2015). TGF-beta Blockade Reduces Mortality and Metabolic Changes in a Validated Murine Model of Pancreatic Cancer Cachexia. *PLoS One, 10*(7), e0132786. doi:10.1371/journal.pone.0132786

Grotendorst, G. R., Smale, G., & Pencev, D. (1989). Production of transforming growth factor beta by human peripheral blood monocytes and neutrophils. *J Cell Physiol, 140*(2), 396-402. doi:10.1002/jcp.1041400226

Hardy, D., Besnard, A., Latil, M., Jouvion, G., Briand, D., Thepenier, C., . . . Chretien, F. (2016). Comparative Study of Injury Models for Studying Muscle Regeneration in Mice. *PLoS One, 11*(1), e0147198. doi:10.1371/journal.pone.0147198

Hennebry, A., Berry, C., Siriett, V., O'Callaghan, P., Chau, L., Watson, T., . . . Kambadur, R. (2009). Myostatin regulates fiber-type composition of skeletal muscle by regulating MEF2 and MyoD gene expression. *Am J Physiol Cell Physiol, 296*(3), C525-534. doi:10.1152/ajpcell.00259.2007

Hillege, M. M. G., Galli Caro, R. A., Offringa, C., de Wit, G. M. J., Jaspers, R. T., & Hoogaars, W. M. H. (2020). TGF-beta Regulates Collagen Type I Expression in Myoblasts and Myotubes via Transient Ctgf and Fgf-2 Expression. *Cells, 9*(2). doi:10.3390/cells9020375

Hock, M. B., & Kralli, A. (2009). Transcriptional control of mitochondrial biogenesis and function. *Annu Rev Physiol, 71*, 177-203. doi:10.1146/annurev.physiol.010908.163119

Hu, J. M., Liu, K., Liu, J. H., Jiang, X. L., Wang, X. L., Chen, Y. Z., . . . Li, F. (2017). CD163 as a marker of M2 macrophage, contribute to predicte aggressiveness and prognosis of Kazakh esophageal squamous cell carcinoma. *Oncotarget, 8*(13), 21526-21538. doi:10.18632/oncotarget.15630

Ishido, M., & Kasuga, N. (2011). In situ real-time imaging of the satellite cells in rat intact and injured soleus muscles using quantum dots. *Histochem Cell Biol, 135*(1), 21-26. doi:10.1007/s00418-010-0767-x

Kaariainen, M., Jarvinen, T., Jarvinen, M., Rantanen, J., & Kalimo, H. (2000). Relation between myofibers and connective tissue during muscle injury repair. *Scand J Med Sci Sports, 10*(6), 332-337. doi:10.1034/j.1600-0838.2000.010006332.x

Kehrl, J. H., Wakefield, L. M., Roberts, A. B., Jakowlew, S., Alvarez-Mon, M., Derynck, R., . . . Fauci, A. S. (1986). Production of transforming growth factor beta by human T lymphocytes and its potential role in the regulation of T cell growth. *J Exp Med, 163*(5), 1037-1050. doi:10.1084/jem.163.5.1037

Kemaladewi, D. U., de Gorter, D. J., Aartsma-Rus, A., van Ommen, G. J., ten Dijke, P., t Hoen, P. A., & Hoogaars, W. M. (2012). Cell-type specific regulation of myostatin signaling. *FASEB J, 26*(4), 1462-1472. doi:10.1096/fj.11-191189

Kotiadis, V. N., Duchen, M. R., & Osellame, L. D. (2014). Mitochondrial quality control and communications with the nucleus are important in maintaining mitochondrial function and cell health. *Biochim Biophys Acta, 1840*(4), 1254-1265. doi:10.1016/j.bbagen.2013.10.041

Langley, B., Thomas, M., Bishop, A., Sharma, M., Gilmour, S., & Kambadur, R. (2002). Myostatin inhibits myoblast differentiation by down-regulating MyoD expression. *J Biol Chem, 277*(51), 49831-49840. doi:10.1074/jbc.M204291200

Larsson, J., Goumans, M. J., Sjostrand, L. J., van Rooijen, M. A., Ward, D., Leveen, P., . . . Karlsson, S. (2001). Abnormal angiogenesis but intact hematopoietic potential in TGF-beta type I receptor-deficient mice. *EMBO J, 20*(7), 1663-1673. doi:10.1093/emboj/20.7.1663

Latres, E., Mastaitis, J., Fury, W., Miloscio, L., Trejos, J., Pangilinan, J., . . . Gromada, J. (2017). Activin A more prominently regulates muscle mass in primates than does GDF8. *Nat Commun, 8*, 15153. doi:10.1038/ncomms15153

Latres, E., Pangilinan, J., Miloscio, L., Bauerlein, R., Na, E., Potocky, T. B., . . . Stitt, T. (2015). Myostatin blockade with a fully human monoclonal antibody induces muscle hypertrophy and reverses muscle atrophy in young and aged mice. *Skelet Muscle, 5*, 34. doi:10.1186/s13395-015-0060-8

Lawrence, D. A., Pircher, R., Kryceve-Martinerie, C., & Jullien, P. (1984). Normal embryo fibroblasts release transforming growth factors in a latent form. *J Cell Physiol, 121*(1), 184-188. doi:10.1002/jcp.1041210123

Lee, S. J., Huynh, T. V., Lee, Y. S., Sebald, S. M., Wilcox-Adelman, S. A., Iwamori, N., . . . Fan, C. M. (2012). Role of satellite cells versus myofibers in muscle hypertrophy induced by inhibition of the myostatin/activin signaling pathway. *Proc Natl Acad Sci U S A, 109*(35), E2353-2360. doi:10.1073/pnas.1206410109

Lee, S. J., Lee, Y. S., Zimmers, T. A., Soleimani, A., Matzuk, M. M., Tsuchida, K., . . . Barton, E. R. (2010). Regulation of muscle mass by follistatin and activins. *Mol Endocrinol, 24*(10), 1998-2008. doi:10.1210/me.2010-0127

Lee, S. J., Lehar, A., Liu, Y., Ly, C. H., Pham, Q. M., Michaud, M., . . . Rando, T. A. (2020). Functional redundancy of type I and type II receptors in the regulation of skeletal muscle growth by myostatin and activin A. *Proc Natl Acad Sci U S A, 117*(49), 30907-30917. doi:10.1073/pnas.2019263117

Lefaucheur, J. P., & Sebille, A. (1995). Muscle regeneration following injury can be modified in vivo by immune neutralization of basic fibroblast growth factor, transforming growth factor beta 1 or insulin-like growth factor I. *J Neuroimmunol, 57*(1-2), 85-91. doi:10.1016/0165-5728(94)00166-l

Leger, B., Derave, W., De Bock, K., Hespel, P., & Russell, A. P. (2008). Human sarcopenia reveals an increase in SOCS-3 and myostatin and a reduced efficiency of Akt phosphorylation. *Rejuvenation Res, 11*(1), 163-175B. doi:10.1089/rej.2007.0588

Lepper, C., Partridge, T. A., & Fan, C. M. (2011). An absolute requirement for Pax7-positive satellite cells in acute injury-induced skeletal muscle regeneration. *Development, 138*(17), 3639-3646. doi:10.1242/dev.067595

Li, Y., Foster, W., Deasy, B. M., Chan, Y., Prisk, V., Tang, Y., . . . Huard, J. (2004). Transforming growth factor-beta1 induces the differentiation of myogenic cells into fibrotic cells in injured skeletal muscle: a key event in muscle fibrogenesis. *Am J Pathol, 164*(3), 1007-1019. doi:10.1016/s0002-9440(10)63188-4

Li, Z. B., Kollias, H. D., & Wagner, K. R. (2008). Myostatin directly regulates skeletal muscle fibrosis. *J Biol Chem, 283*(28), 19371-19378. doi:10.1074/jbc.M802585200

Lindstrom, M., & Thornell, L. E. (2009). New multiple labelling method for improved satellite cell identification in human muscle: application to a cohort of power-lifters and sedentary men. *Histochem Cell Biol, 132*(2), 141-157. doi:10.1007/s00418-009-0606-0

Liu, D., Black, B. L., & Derynck, R. (2001). TGF-beta inhibits muscle differentiation through functional repression of myogenic transcription factors by Smad3. *Genes Dev, 15*(22), 2950-2966. doi:10.1101/gad.925901

Mahdy, M. A., Lei, H. Y., Wakamatsu, J., Hosaka, Y. Z., & Nishimura, T. (2015). Comparative study of muscle regeneration following cardiotoxin and glycerol injury. *Ann Anat, 202*, 18-27. doi:10.1016/j.aanat.2015.07.002

Mathew, S. J., Hansen, J. M., Merrell, A. J., Murphy, M. M., Lawson, J. A., Hutcheson, D. A., . . . Kardon, G. (2011). Connective tissue fibroblasts and Tcf4 regulate myogenesis. *Development, 138*(2), 371-384. doi:10.1242/dev.057463

McCarthy, J. J., Srikuea, R., Kirby, T. J., Peterson, C. A., & Esser, K. A. (2012a). Correction: Inducible Cre transgenic mouse strain for skeletal muscle-specific gene targeting. *Skelet Muscle, 2*(1), 22. doi:10.1186/2044-5040-2-22

McCarthy, J. J., Srikuea, R., Kirby, T. J., Peterson, C. A., & Esser, K. A. (2012b). Inducible Cre transgenic mouse strain for skeletal muscle-specific gene targeting. *Skelet Muscle, 2*(1), 8. doi:10.1186/2044-5040-2-8

McCroskery, S., Thomas, M., Platt, L., Hennebry, A., Nishimura, T., McLeay, L., . . . Kambadur, R. (2005). Improved muscle healing through enhanced regeneration and reduced fibrosis in myostatin-null mice. *J Cell Sci, 118*(Pt 15), 3531-3541. doi:10.1242/jcs.02482

McFarlane, C., Plummer, E., Thomas, M., Hennebry, A., Ashby, M., Ling, N., . . . Kambadur, R. (2006). Myostatin induces cachexia by activating the ubiquitin proteolytic system through an NF-kappaB-independent, FoxO1-dependent mechanism. *J Cell Physiol, 209*(2), 501-514. doi:10.1002/jcp.20757

Mendias, C. L., Gumucio, J. P., Davis, M. E., Bromley, C. W., Davis, C. S., & Brooks, S. V. (2012). Transforming growth factor-beta induces skeletal muscle atrophy and fibrosis through the induction of atrogin-1 and scleraxis. *Muscle Nerve, 45*(1), 55-59. doi:10.1002/mus.22232

Miller, K. J., Thaloor, D., Matteson, S., & Pavlath, G. K. (2000). Hepatocyte growth factor affects satellite cell activation and differentiation in regenerating skeletal muscle. *Am J Physiol Cell Physiol, 278*(1), C174-181. doi:10.1152/ajpcell.2000.278.1.C174

Mosser, D. M., & Edwards, J. P. (2008). Exploring the full spectrum of macrophage activation. *Nat Rev Immunol, 8*(12), 958-969. doi:10.1038/nri2448

Murach, K. A., Englund, D. A., Dupont-Versteegden, E. E., McCarthy, J. J., & Peterson, C. A. (2018). Myonuclear Domain Flexibility Challenges Rigid Assumptions on Satellite Cell Contribution to Skeletal Muscle Fiber Hypertrophy. *Front Physiol, 9*, 635. doi:10.3389/fphys.2018.00635

Murphy, K. T., Chee, A., Gleeson, B. G., Naim, T., Swiderski, K., Koopman, R., & Lynch, G. S. (2011). Antibody-directed myostatin inhibition enhances muscle mass and function

in tumor-bearing mice. *Am J Physiol Regul Integr Comp Physiol, 301*(3), R716-726. doi:10.1152/ajpregu.00121.2011

Murphy, M. M., Lawson, J. A., Mathew, S. J., Hutcheson, D. A., & Kardon, G. (2011). Satellite cells, connective tissue fibroblasts and their interactions are crucial for muscle regeneration. *Development, 138*(17), 3625-3637. doi:10.1242/dev.064162

Narola, J., Pandey, S. N., Glick, A., & Chen, Y. W. (2013). Conditional expression of TGF-beta1 in skeletal muscles causes endomysial fibrosis and myofibers atrophy. *PLoS One, 8*(11), e79356. doi:10.1371/journal.pone.0079356

Novak, M. L., Weinheimer-Haus, E. M., & Koh, T. J. (2014). Macrophage activation and skeletal muscle healing following traumatic injury. *J Pathol, 232*(3), 344-355. doi:10.1002/path.4301

Pedersen, B. K., Steensberg, A., & Schjerling, P. (2001). Exercise and interleukin-6. *Curr Opin Hematol, 8*(3), 137-141. doi:10.1097/00062752-200105000-00002

Perdomo, G., Martinez-Brocca, M. A., Bhatt, B. A., Brown, N. F., O'Doherty, R. M., & Garcia-Ocana, A. (2008). Hepatocyte growth factor is a novel stimulator of glucose uptake and metabolism in skeletal muscle cells. *J Biol Chem, 283*(20), 13700-13706. doi:10.1074/jbc.M707551200

Rebbapragada, A., Benchabane, H., Wrana, J. L., Celeste, A. J., & Attisano, L. (2003). Myostatin signals through a transforming growth factor beta-like signaling pathway to block adipogenesis. *Mol Cell Biol, 23*(20), 7230-7242. doi:10.1128/mcb.23.20.7230-7242.2003

Reibman, J., Meixler, S., Lee, T. C., Gold, L. I., Cronstein, B. N., Haines, K. A., . . . Weissmann, G. (1991). Transforming growth factor beta 1, a potent chemoattractant for human neutrophils, bypasses classic signal-transduction pathways. *Proc Natl Acad Sci U S A, 88*(15), 6805-6809. doi:10.1073/pnas.88.15.6805

Ripoche, D., Gout, J., Pommier, R. M., Jaafar, R., Zhang, C. X., Bartholin, L., & Bertolino, P. (2013). Generation of a conditional mouse model to target Acvr1b disruption in adult tissues. *Genesis, 51*(2), 120-127. doi:10.1002/dvg.22352

Rivero, J. L., Talmadge, R. J., & Edgerton, V. R. (1998). Fibre size and metabolic properties of myosin heavy chain-based fibre types in rat skeletal muscle. *J Muscle Res Cell Motil, 19*(7), 733-742. doi:10.1023/a:1005482816442

Sartori, R., Gregorevic, P., & Sandri, M. (2014). TGFbeta and BMP signaling in skeletal muscle: potential significance for muscle-related disease. *Trends Endocrinol Metab, 25*(9), 464-471. doi:10.1016/j.tem.2014.06.002

Sartori, R., Milan, G., Patron, M., Mammucari, C., Blaauw, B., Abraham, R., & Sandri, M. (2009). Smad2 and 3 transcription factors control muscle mass in adulthood. *Am J Physiol Cell Physiol, 296*(6), C1248-1257. doi:10.1152/ajpcell.00104.2009

Schaer, D. J., Boretti, F. S., Hongegger, A., Poehler, D., Linnscheid, P., Staege, H., . . . Schaffner, A. (2001). Molecular cloning and characterization of the mouse CD163 homologue, a highly glucocorticoid-inducible member of the scavenger receptor cysteine-rich family. *Immunogenetics, 53*(2), 170-177. doi:10.1007/s002510100304

Schneider, C. A., Rasband, W. S., & Eliceiri, K. W. (2012). NIH Image to ImageJ: 25 years of image analysis. *Nat Methods, 9*(7), 671-675. doi:10.1038/nmeth.2089

Schultz, E., Jaryszak, D. L., & Valliere, C. R. (1985). Response of satellite cells to focal skeletal muscle injury. *Muscle Nerve, 8*(3), 217-222. doi:10.1002/mus.880080307

Serrano, A. L., Baeza-Raja, B., Perdiguero, E., Jardi, M., & Munoz-Canoves, P. (2008). Interleukin-6 is an essential regulator of satellite cell-mediated skeletal muscle hypertrophy. *Cell Metab, 7*(1), 33-44. doi:10.1016/j.cmet.2007.11.011

Smith, L. R., & Barton, E. R. (2014). SMASH - semi-automatic muscle analysis using segmentation of histology: a MATLAB application. *Skelet Muscle, 4*, 21. doi:10.1186/2044-5040-4-21

Smith, M. J., & Koch, G. L. (1987). Differential expression of murine macrophage surface glycoprotein antigens in intracellular membranes. *J Cell Sci, 87 (Pt 1)*, 113-119. Retrieved from https://www.ncbi.nlm.nih.gov/pubmed/3312248

Tanaka, M., Miyazaki, H., Takeda, Y., & Takeo, S. (1993). Detection of serum cytokine levels in experimental cancer cachexia of colon 26 adenocarcinoma-bearing mice. *Cancer Lett, 72*(1-2), 65-70. doi:10.1016/0304-3835(93)90012-x

Tatsumi, R., Anderson, J. E., Nevoret, C. J., Halevy, O., & Allen, R. E. (1998). HGF/SF is present in normal adult skeletal muscle and is capable of activating satellite cells. *Dev Biol, 194*(1), 114-128. doi:10.1006/dbio.1997.8803

ten Dijke, P., Yamashita, H., Ichijo, H., Franzen, P., Laiho, M., Miyazono, K., & Heldin, C. H. (1994). Characterization of type I receptors for transforming growth factor-beta and activin. *Science, 264*(5155), 101-104. doi:10.1126/science.8140412

Tidball, J. G. (2017). Regulation of muscle growth and regeneration by the immune system. *Nat Rev Immunol, 17*(3), 165-178. doi:10.1038/nri.2016.150

Trendelenburg, A. U., Meyer, A., Jacobi, C., Feige, J. N., & Glass, D. J. (2012). TAK-1/p38/nNFkappaB signaling inhibits myoblast differentiation by increasing levels of Activin A. *Skelet Muscle, 2*(1), 3. doi:10.1186/2044-5040-2-3

Trendelenburg, A. U., Meyer, A., Rohner, D., Boyle, J., Hatakeyama, S., & Glass, D. J. (2009). Myostatin reduces Akt/TORC1/p70S6K signaling, inhibiting myoblast differentiation and myotube size. *Am J Physiol Cell Physiol, 296*(6), C1258-1270. doi:10.1152/ajpcell.00105.2009

Tsuchida, K., Nakatani, M., Uezumi, A., Murakami, T., & Cui, X. (2008). Signal transduction pathway through activin receptors as a therapeutic target of musculoskeletal diseases and cancer. *Endocr J, 55*(1), 11-21. doi:10.1507/endocrj.kr-110

Tsunawaki, S., Sporn, M., Ding, A., & Nathan, C. (1988). Deactivation of macrophages by transforming growth factor-beta. *Nature, 334*(6179), 260-262. doi:10.1038/334260a0

van der laarse, W., Tombe, A. L., Groot, M. B. E., & Diegenbach, P. C. (1997). Size Principle of Striated Muscle Cells. *Netherlands Journal of Zoology, 48*, 213-223. doi:10.1163/156854298X00075

van der Laarse, W. J., Diegenbach, P. C., & Elzinga, G. (1989). Maximum rate of oxygen consumption and quantitative histochemistry of succinate dehydrogenase in single muscle fibres of Xenopus laevis. *J Muscle Res Cell Motil, 10*(3), 221-228. doi:10.1007/BF01739812

van der Meer, S. F., Jaspers, R. T., Jones, D. A., & Degens, H. (2011). The time course of myonuclear accretion during hypertrophy in young adult and older rat plantaris muscle. *Ann Anat, 193*(1), 56-63. doi:10.1016/j.aanat.2010.08.004

van Wessel, T., de Haan, A., van der Laarse, W. J., & Jaspers, R. T. (2010). The muscle fiber type-fiber size paradox: hypertrophy or oxidative metabolism? *Eur J Appl Physiol, 110*(4), 665-694. doi:10.1007/s00421-010-1545-0

Verbrugge, S. A. J., Gehlert, S., Stadhouders, L. E. M., Jacko, D., Aussieker, T., G, M. J. d. W., . . . Wackerhage, H. (2020). PKM2 Determines Myofiber Hypertrophy In Vitro and Increases in Response to Resistance Exercise in Human Skeletal Muscle. *Int J Mol Sci, 21*(19). doi:10.3390/ijms21197062

Wahl, S. M., Hunt, D. A., Wakefield, L. M., McCartney-Francis, N., Wahl, L. M., Roberts, A. B., & Sporn, M. B. (1987). Transforming growth factor type beta induces monocyte chemotaxis and growth factor production. *Proc Natl Acad Sci U S A, 84*(16), 5788-5792. doi:10.1073/pnas.84.16.5788

Wiseman, D. M., Polverini, P. J., Kamp, D. W., & Leibovich, S. J. (1988). Transforming growth factor-beta (TGF beta) is chemotactic for human monocytes and induces their expression of angiogenic activity. *Biochem Biophys Res Commun, 157*(2), 793-800. doi:10.1016/s0006-291x(88)80319-x

Wu, X., Zhao, J., Cui, X. L., Li, Q., Tao, H., Pan, Q. J., . . . Li, M. Q. (2017). [Prevalence of type-specific human papillomavirus infection among 18-45 year-old women from the general population in Liuzhou, Guangxi Zhuang Autonomous Region: a cross-sectional study]. *Zhonghua Liu Xing Bing Xue Za Zhi, 38*(4), 467-471. doi:10.3760/cma.j.issn.0254-6450.2017.04.011

Yang, S. Y., & Goldspink, G. (2002). Different roles of the IGF-I Ec peptide (MGF) and mature IGF-I in myoblast proliferation and differentiation. *FEBS Lett, 522*(1-3), 156-160. doi:10.1016/s0014-5793(02)02918-6

Zhang, C., Li, Y., Wu, Y., Wang, L., Wang, X., & Du, J. (2013). Interleukin-6/signal transducer and activator of transcription 3 (STAT3) pathway is essential for macrophage infiltration and myoblast proliferation during muscle regeneration. *J Biol Chem, 288*(3), 1489-1499. doi:10.1074/jbc.M112.419788

Zimmers, T. A., Davies, M. V., Koniaris, L. G., Haynes, P., Esquela, A. F., Tomkinson, K. N., . . . Lee, S. J. (2002). Induction of cachexia in mice by systemically administered myostatin. *Science, 296*(5572), 1486-1488. doi:10.1126/science.1069525

Zimowska, M., Duchesnay, A., Dragun, P., Oberbek, A., Moraczewski, J., & Martelly, I. (2009). Immunoneutralization of TGFbeta1 Improves Skeletal Muscle Regeneration: Effects on Myoblast Differentiation and Glycosaminoglycan Content. *Int J Cell Biol, 2009*, 659372. doi:10.1155/2009/659372

1369

1370

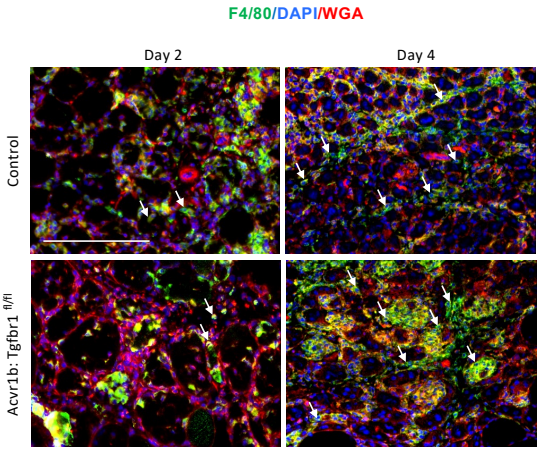

1371

1372 Figure 5-figure supplement 1. Number of macrophages in TA of Acvr1b$^{fl/fl}$:Tgfbr1$^{fl/fl}$
1373 animals was increased 4 days post injury. Number of macrophages (F4/80^{+}, green) in
1374 control and Acvr1b$^{fl/fl}$:Tgfbr1$^{fl/fl}$ animals on day 2 and 4 post injury. Nuclei were stained
1375 by DAPI (blue) and ECM of muscle were stained by WGA (red). Scale bar=100 µm.
1376 N=5-7.
1377

1378

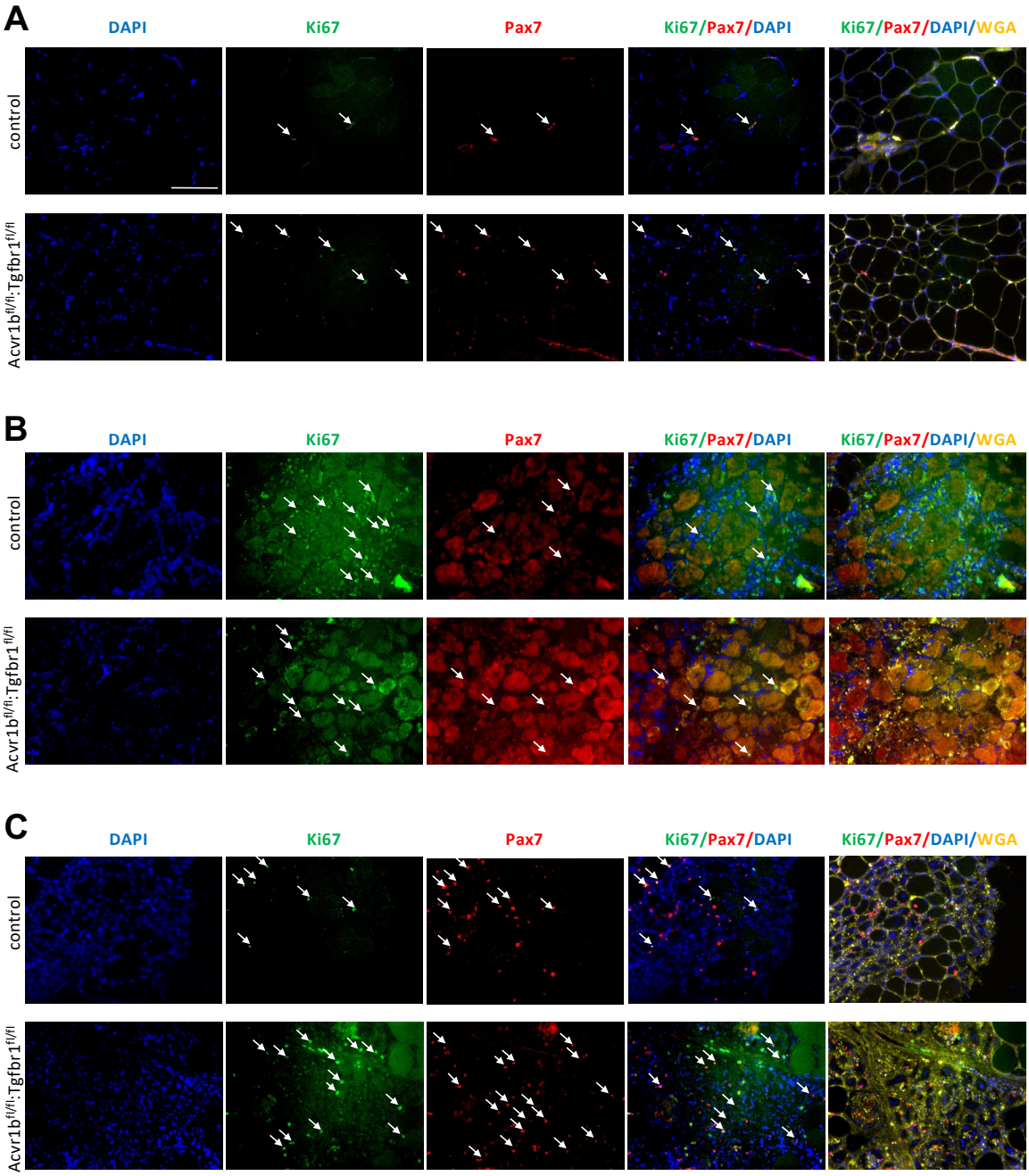

Figure 5-figure supplement 2. Increased number of proliferating cells and satellite cells in TA of Acvr1b$^{fl/fl}$: Tgfbr1$^{fl/fl}$ animals in absence of injury and 4 days post injury. (A) In absence of injury, proliferating cells (Ki67^{+}, green, white arrows) and muscle satellite cells (Pax7^{+}, red, white arrows) were shown by IF staining in low oxidative area of TA, where regeneration patches were found. Two (B) and 4 (C) days post injury, more Ki67^{+} and Pax7^{+} cells (white arrows) infiltrated in injured area. Nuclei were stained by DAPI (blue) and ECM of muscle were stained by WGA (yellow). Scale bar=100 μm. N=5-7.

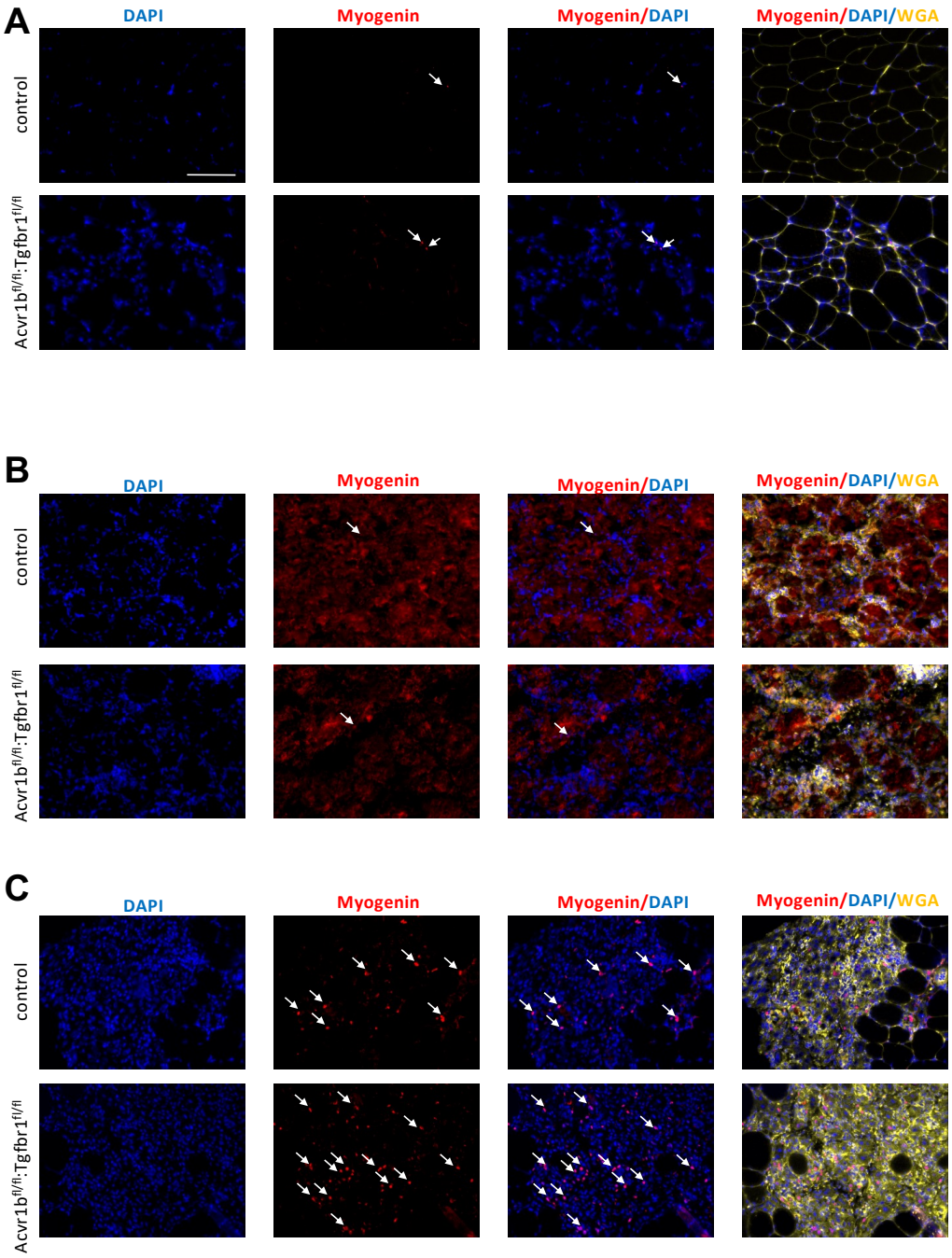

Figure 5-figure supplement 3. Increased number of differentiating muscle cells in TA of Acvr1b$^{fl/fl}$: Tgfbr1$^{fl/fl}$ animals 4 days post injury. On day 0 (A) and 2 days (B) post injury, number of differentiating myoblasts (myogenin^{+}, red, white arrows) was of no difference between groups. Four days (C) post injury, more Myogenin^{+} cells were found in injured area of Acvr1b$^{fl/fl}$: Tgfbr1$^{fl/fl}$ animals. Nuclei were stained by DAPI (blue) and ECM of muscle were stained by WGA (yellow). Scale bar=100 μm. N=5-7.